International Journal of Nanomedicine

Dovepress
Taylor & Francis Group

Open Access Full Text Article

ORIGINAL RESEARCH

MSN Templated with L-Dopa Amide Derivatives Outperforms the Efficiency of Free-L-Dopa in Reducing Parkinson's Behavioral Dysfunction in Mice

Mónica Onrubia-Márquez[1], Miguel M Garcia[2–4], Francisco Navas[1], Samuel Martínez-Erro[1], Antonio Martín[1], Victoria Morales[1], Justine Delaval[5], Lara Merchán-Sánchez[6], Eva Mª Sánchez-Robles[2–4], Nancy A Paniagua[2–4], Carmen Rodríguez-Rivera[2–4], Raúl Sanz[1,7], Carlos Goicoechea[2–4], Rafael A García-Muñoz[1,7]

[1]Department of Chemical and Environmental Technology, Universidad Rey Juan Carlos, Móstoles, Spain; [2]Area of Pharmacology, Nutrition and Bromatology, Department of Basic Health Sciences, Universidad Rey Juan Carlos, Unidad Asociada de I+D+i Al Instituto de Química Médica (IQM) CSIC-URJC, Alcorcón, Spain; [3]High Performance Experimental Pharmacology Research Group, Universidad Rey Juan Carlos (PHARMAKOM), Alcorcón, Spain; [4]Grupo Multidisciplinar de Investigación y Tratamiento del Dolor (i+DOL), Alcorcón, Spain; [5]École de Biologie Industrielle (EBI), Cergy, France; [6]Area of Histology and Pathological Anatomy, Department of Basic Health Sciences, Universidad Rey Juan Carlos, Alcorcón, Spain; [7]Instituto de Investigación de Tecnologías para la Sostenibilidad, Universidad Rey Juan Carlos, Móstoles, Spain

Correspondence: Victoria Morales; Rafael A García-Muñoz, Email victoria.morales@urjc.es; rafael.garcia@urjc.es

Introduction: Parkinson's disease (PD) is a progressive neurodegenerative disorder characterized by motor dysfunction due to the loss of dopaminergic neurons, with an increasing global prevalence estimated to impact 20 million individuals by 2050. The current standard treatment, L-dopa, loses efficacy over time and often induces dyskinesia, highlighting the need for innovative therapeutic strategies with sustained efficacy and fewer side effects.

Methods: In this study, we developed mesoporous silica nanoparticles (MSNs) templated with L-dopa amide derivatives, specifically designed as a drug-structure-directing agent (DSDA). This novel templating approach improves L-dopa loading capacity and enhances controlled-release performance. Two MSN formulations were selected for in vivo evaluation in a murine model of PD induced by unilateral injection of 6-hydroxydopamine (6-OHDA) in the striatum.

Results: In vitro studies demonstrated that L-dopa derivatives-loaded MSNs lead to a controlled and sustained release of L-dopa DSDA and in vivo assays corroborated this hypothesis. A single intraperitoneal dose of L-dopa-loaded MSNs was able to reduce the spontaneous rotational behavior observed in 6-OHDA damaged mice and outdid free-L-dopa.

Conclusion: This novel strategy may represent a promising alternative to conventional treatment, reducing dose frequency and hence minimizing L-dopa side effects. The results herein emphasize the potential of MSN-based drug delivery systems for PD, providing a basis for future translational research of nanotechnology-based formulations for neurodegenerative disorders.

Keywords: Parkinson disease, mesoporous silica nanoparticles, modified L-Dopa, drug-structure-directing agents, drug release systems

Introduction

Neurodegenerative diseases are among one of the leading causes of disability worldwide.[1] These relatively common chronic disorders affect the central nervous system, with the accumulation of protein aggregates as a frequent hallmark.[2] Parkinson's disease (PD), the second-most common neurodegenerative disease,[3,4] typically accumulates truncated and phosphorylated α-synuclein protein aggregates[5,6] that ultimately cause alterations of cellular processes involved in normal cell functioning leading to apoptosis of the neuron or glial cell. These include the autophagy lysosomal pathway, mitochondrial function, endoplasmic reticulum stress sensing and signaling mechanisms, and the activation of cellular responses to protein misfolding or the vesicular transport. This is particularly evident in the substantia nigra, a midbrain

https://doi.org/10.2147/IJN.S545116
Received: 5 June 2025
Accepted: 9 December 2025
Published: 12 February 2026

Graphical Abstract

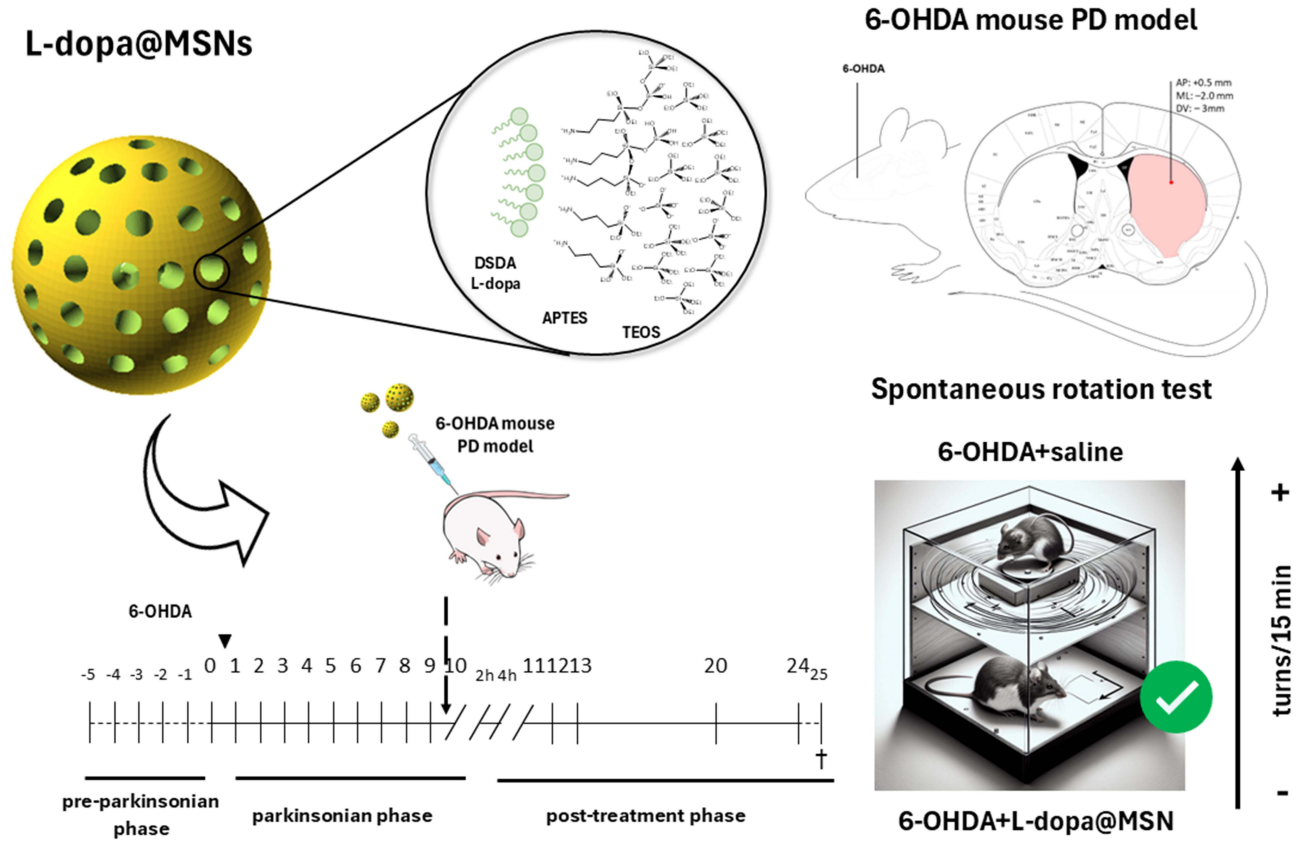

dopaminergic nucleus that plays a pivotal role in regulating motor movement and reward functions.[7,8] Hence, the associated symptoms typically include the presence of bradykinesia, rigidity, impaired body rotation and rest tremors as well as non-locomotor symptoms such as constipation, depression, and sleep disorders.[9,10]

After sixty years, L-dopa (L-3,4-dihydroxyphenylalanine) remains the most effective drug for the management of motor symptoms of Parkinson's disease yet no cure available.[11] Unlike dopamine, L-dopa can cross the blood–brain barrier via the LAT-1 transporter. Once inside the brain, this prodrug is converted into dopamine, alleviating some of the symptoms associated with the disease. Dopaminergic agonists, such as pramipexole and ropinirole, represent an alternative pharmacological strategy based on the stimulation of dopamine receptors to enhance dopaminergic activity. Although these drugs generally exhibit a longer half-life than L-dopa, their efficacy is usually lower; therefore, they are mainly used as adjunct or alternative therapies to mitigate the adverse effects of conventional treatment.[12] However, chronic administration of L-dopa is associated with the development of adverse events including motor impairment and fluctuations, and autonomic symptoms.[13,14] The causes beneath can be manifold, but its short plasma half-life (0.6–-1.3 hours) and a variable gastrointestinal absorption may explain variations in plasma levels and treatment response.[7]

To overcome these limitations new approaches are being investigated.[15] The use of carbidopa (Scheme S1) as an adjuvant peripheral enzymatic inhibitor and gel formulations have shown to improve L-dopa's half-life (half-life is increased to approximately 1.5 hours) and peak-valley fluctuations.[16] A novel subcutaneous L-dopa/carbidopa device has been developed to achieve a continuous release of L-dopa and avoid plasma drug fluctuation. In clinical trials, this device showed an improvement in response to treatment.[17] Another study tested a gel infusion of L-dopa/carbidopa in 24 patients with dyskinesia. Subjects experienced improvements not only in motor symptoms but also in mood and

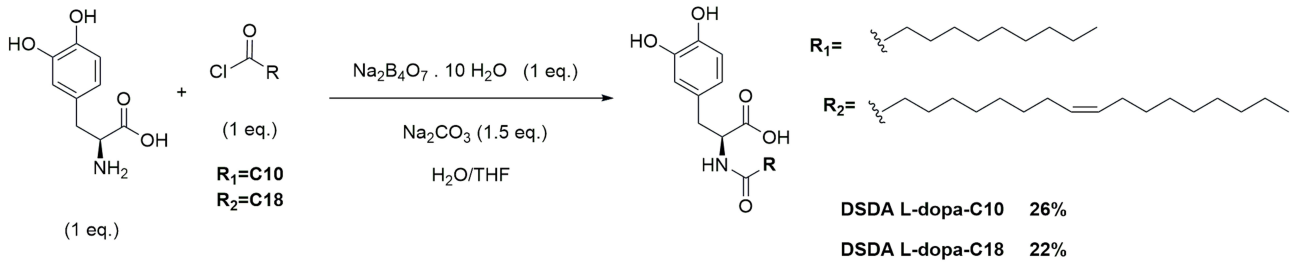

Scheme 1 Synthesis of DSDA L-dopa-C10 and L-dopa-C18.

anxiety.[18] Taken together, these studies suggest that new forms of sustained delivery of L-dopa may be a good approach to avoiding the unwanted side effects of the drug.[19]

In the last years, nanomedicine has emerged as a promising tool for controlled drug release. Drug delivery systems (DDS) allow for long-distance transport to reach specific targets, reducing drug exposure and minimizing toxicity and side effects. The therapeutic profile of the drug is also improved. In this regard, previous works have shown safety and stability profiles when encapsulating dopamine[20] and L-dopa/carbidopa in polymeric nanoparticles.[21] Recently, the neuroprotective effects of L-dopa-modified zinc oxide nanoparticles in PD rat model are evaluated.[22] Among the different DDSs, mesoporous silica nanoparticles (MSNs) have received much attention in recent years due to their outstanding features. Their unique properties include large surface areas and modifiable pore sizes (between 2–50 nm), which are suitable for accommodating the drug inside.[23–25] These DDS may lead to an improvement in drug delivery by providing a prolonged release that may result in increased therapeutic efficacy.[26] In other cases, MSNs act as an efficient encapsulation method, releasing the drug at the therapeutic target.[27] Moreover, these materials have shown to be biocompatible and do not present any problems of toxicity once inside the body.[23,28] In a typical synthesis of MSNs as DDS, an amphiphilic surfactant is used as a template, which is then removed, leaving empty pores available for drug loading. Drug encapsulation is typically achieved by adsorption onto the silica surface.[29–32] Most research has been focused on modifying the silica surface and pore size to improve the affinity between the nanovehicle host and the drug candidate to avoid the undesirable premature release of the drug.[33,34] Usually, these modifications consist in changing surface polarity introducing new functionalities onto the silica surface or using pore expander compounds in the synthesis to obtain large-pore templated silica.[31,35,36] However, premature release is still present in these modified materials.[37] Careful attention must be paid to the design of nanomedicine in order to allow blood–brain barrier (BBB) crossing, as this is one of the main limitations for targeting the central nervous system (CNS). MSNs have been widely used to achieve long-circulating vehicles for drugs and enhance permeabilization of biological barriers. Several reports have highlighted this issue and indicate that size and shape of nanoparticles have a critical role in their biodistribution and excretion.[25,38–40] The effect of several sizes of MSNs on BBB permeability has been evaluated, showing size-dependent behavior. Although there is no consensus on the optimal size, nanoparticles smaller than 100 nm have been found to cross the BBB.[41–43] MSNs offer high surface area and tunable mesopores that enable efficient loading and controlled, sustained release of L-dopa, helping to stabilize plasma exposure and mitigate premature metabolism. Through particle-size control and rational surface chemistry, MSNs can be engineered to improve circulation and facilitate interaction with the blood–brain barrier (BBB). Unlike immediate-release oral L-dopa (typically co-formulated with carbidopa), which shows short half-life and substantial peripheral conversion, MSNs can physically confine drug cargo within mesopores and release it gradually, potentially supporting more consistent CNS exposure.

Although MSNs have many advantages over other DDSs, there are only a few examples of L-dopa-loaded MSNs described in the literature.[44–47] Our group has developed a new strategy to synthesize MSNs, introducing the concept of drug-structure-directing agent (DSDA) based on the use of lipid derivative molecules with pharmacological activity as templates. The DSDA is obtained by the amidation of the drug with a fatty acid, which allows the formation of micelles around which the inorganic silica species self-assemble to form MSNs. This new approach eliminates the need for surfactant removal following MSN formation, as the surfactant itself exhibits inherent pharmacological activity.[48,49] Interestingly, in vitro experiments reveal an improvement in the sustained release capacity and therapeutic effect of

MSNs compared to conventional drug loading methods.[50–54] Moreover, since this strategy relies on the incorporation of an alkyl chain into the therapeutic molecule, its lipophilicity is increased, potentially enhancing the drug's ability to cross the BBB. Consequently, the therapeutic agent could traverse the BBB either through the influence of MSN size and morphology or as a result of increased hydrophobicity and higher blood concentration due to the continuous release.

This study investigates the potential of MSNs templated with L-dopa amide derivatives as a novel therapeutic approach for Parkinson's disease. The primary objective was to synthetize MSNs with the desired characteristics to target CNS and achieve a sustained L-dopa release profile. To this end, we optimized synthesis parameters (including aliphatic chain length, DSDA:water ratio, synthesis temperature, and time) to obtain nanoparticles with an optimal size and maximize L-dopa loading. In vitro drug release assays were conducted to evaluate whether the DSDA strategy enables prolonged drug release, in comparison to conventional adsorption methods. Finally, in vivo behavioral studies were performed to assess whether the sustained release correlates with therapeutic efficacy. Two MSNs (templated with decanoyl (C10) and oleoyl (C18) L-dopa amide derivatives) were selected for in vivo testing in a 6-OHDA-induced mouse model of Parkinson's disease via unilateral injection of 6-OHDA in the striatum, a well-established model that replicates the nigrostriatal degeneration characteristic of the disease. The selection of L-dopa derivatives with decanoyl (C10) and oleoyl (C18) chains was based on their differing hydrophobicity and micelle-forming capabilities, which influence nanoparticle formation, size, drug loading, and release kinetics. These two derivatives were selected to evaluate the impact of alkyl chain length on in vivo behavior and therapeutic outcomes. Behavioral performance was monitored to quantify locomotor activity following administration of a single dose of L-dopa-loaded MSN and compared to animals treated with free L-dopa.

Materials and Methods

Chemicals

3,4-Dihydroxy-L-phenylalanine (L-dopa, >98%) was purchased from Fisher Scientific; sodium carbonate (99%), and tetrahydrofuran (THF, 99.5%), ethyl acetate (99%), ethanol absolute were purchased from Scharlab (Barcelona, Spain); sodium sulphate anhydrous (99.8%), dicloromethane (CH_2Cl_2, 99.9%), dimethyl sulphoxide (DMSO, 99%) were purchased from QUIMIPUR (Madrid, Spain); methanol (99.9%) was purchased from Honeywell (New Jersey, USA); silica gel was purchased from LabKem (Barcelona, Spain); oleoyl chloride (≥89%), decanoyl chloride (98%), (3-aminopropyl)triethoxysilane (APTES, 98%), (3-aminopropyl)trimethoxysilane (APTMS, 98%), toluene (99%), tetraethylorthosilicate (TEOS, 98%), hydrochloric acid (35% w/w), di-Sodium tetraborate decahydrated ($Na_2B_4O_7{\cdot}10H_2O$, 99.5%), dimethyl sulfoxide-D6 (99.8% D), 3-(4, 5-dimethyl-2-thiazolyl)-2,5-diphenyl-2H-tetrazolium bromide (MTT, 98%), phosphate buffered saline tablets (PBS), Fetal Bovine Serum (FBS), sodium chloride (>99%), 6-hydroxydopamine hydrochloride (6-OHDA, 97%) were obtained from Sigma-Aldrich (Madrid, Spain). Dodecane was purchased from Fluka (New Jersey, USA). The porcine brain lipid (PBL) was obtained from Avanti Polar Lipids (Alabama, USA).

Animals

CD-1® adult mice were purchased from Envigo (Barcelona, Spain). All animals were four weeks old (25–30mg) at the beginning of this study and were housed (4–6 mice/cage) in conventional polycarbonate EU Type 3 cages (height: 150 mm; top size: 425×265 mm; bottom size: 375×215 mm). They were maintained in a temperature (23 ± 1°C) and humidity (50–55%) controlled room, under a 12 h light/dark cycle (lights off between 19:00 and 07.00 h). Animals had free access to standard laboratory rat chow (Envigo) and tap water. Trained investigators blind to drug treatment conducted all the behavioral assays. Experiments were performed between 9:00 a.m. and 12:00 p.m. All animal procedures were designed and conducted in accordance with a protocol approved by the Ethical Committee of Universidad Rey Juan Carlos and by the Autonomous Region of Madrid (PROEX 247.4/22) and followed the guidelines for the Care and Use of Laboratory Animals of the European Union Directive (2010/63/EU) and Spanish regulations (Law 32/2007, RD 53/2013 and order ECC/566/2015). A total of 89 female were utilized to study the effect of long-term treatment of L-dopa@MSNs. Then, a smaller group composed of 12 male mice was used to examine differences related to sex. 7 casualties were encountered. The number of animals used, and their suffering were minimized.

Characterization

^{1}H NMR and ^{13}C NMR spectra were recorded on a Varian Infinity 400 MHz spectrometer (URJC, Móstoles, Spain) fitted with a 9.4 T magnetic field. Chemical shifts are reported in parts per million (δ ppm) and externally referenced to tetramethylsilane. The separation of the synthesized compounds was confirmed by thin-layer chromatography (TLC) on Merck 60 F_{254} silica gel. Mass measurements were performed on an ultra-high-performance liquid chromatography tandem mass spectrometry (UHPLC-HESI-MS/MS) using Vacuum Insulated Probe Heated Electrospray Ionization (Bruker UHPLC/MSMS EVOQ™ ELITE) with a triple-quadrupole detector (URJC, Móstoles, Spain). Nitrogen adsorption measurements were performed on a Micromeritics TriStar 3000 instrument (URJC, Móstoles, Spain). In general, calcinated samples (100 mg) were heated to 100°C for 24 h in vacuum to outgas them before nitrogen sorption measurements. Subsequent nitrogen sorption measurements were performed at 77 K (−196.15°C). Pore size and pore volume were calculated by a non-local density functional theory NLDFT model on the adsorption branch of the isotherms. Thermogravimetric analyses (TGA) were performed under air atmosphere with a Star system Mettler Thermobalance (URJC, Móstoles, Spain) in the temperature range from 40 to 800°C at 5°C min^{-1}. The elemental analysis (EA) was performed using a CHNS-O analyzer Flash 2000 Thermo Scientific apparatus (URJC, Móstoles, Spain). Fourier Transform Infrared Spectroscopy (FTIR) analyses were collected, using attenuated total reflectance technique (ATR), on a Mattson Infinity series apparatus in the wavelength range from 4000 to 400 cm^{-1} with a step size of 2 cm^{-1} and collecting 64 scans for each analysis. The morphologies and sizes of MSNs were investigated with transmission electron microscopy (TEM) JEOL JEM 2100 operated at 200 kV with a resolution of 0.25 nm (Complutense University of Madrid). Previously the samples were dispersed in ethanol and deposited on a carbon-coated copper grid. The size of MSNs by TEM was determined using ImageJ software, with 20 random nanoparticles measured and the result reported as the mean±SD. Dynamic Light Scattering (DLS) measurements were performed on Nanoplus DLS/Zeta Potential from Particulate Systems particulate nanaosystem (URJC, Móstoles, Spain). Samples were suspended in HEPES 1M buffer at pH 7.4 with 0.25 mg mL^{-1} concentration.

Synthesis of Anionic DSDAs L-Dopa

The DSDAs from L-dopa were synthesized through an amidation reaction between decanoyl chloride or alternatively oleoyl chloride and the amino group of the L-dopa moiety (Scheme 1) to obtain N-decanoyl-L-dopa (L-dopa-C10) and N-oleyl-L-dopa (L-dopa-C18), respectively. The reaction was performed according to a modified procedure described in the literature.[52,55] In a round-bottom flask, equipped with a magnetic stirrer, Borax (3.86 g, 10.1 mmol) was dissolved in 100 mL of water. The mixture was degassed for 30 min, followed by the addition of L-dopa (2 g, 10.1 mmol). In order to reach a pH 8–9, sodium carbonate (0.80 g, 7.6 mmol) was finally added to the mixture, which was then degassed for another 5 min. Subsequently, decanoyl or oleoyl chloride (2.13 or 3.3 mL, 10.1 mol) was dissolved in degassed THF (25 mL) and added dropwise to the solution of L-dopa. The mixture was stirred at room temperature for 24 h under inert atmosphere. Following this, the pH was adjusted to 1–2 with hydrochloric acid. The aqueous layer was then extracted with ethyl acetate (3 x 15 mL) and the combined organic layers were washed successively with water (4 x 25 mL) and brine (1 x 25 mL) and dried over anhydrous sodium sulfate. The mixture was filtered, and the solvent removed under reduced pressure. The residue was finally purified by flash column chromatography (silica gel, CH_2Cl_2:Methanol 2%) to obtain the L-dopa DSDA as a sticky brown solid (26–22% yield).

Synthesis of Mesoporous Silica Nanoparticles with DSDA L-Dopa (L-dopa@MSNs)

The synthesis of L-dopa@MSNs was performed using the synthesized anionic DSDAs, N-decanoyl-L-dopa (L-dopa-C10) or alternatively N-oleyl-L-dopa (L-dopa-C18) as surfactant. The reaction was performed according to a protocol developed in our laboratory for the synthesis of MSNs using anionic DSDAs as template.[49,52] Different synthesis parameters were studied to improve the properties of MSNs for in vivo assays. The parameters studied were the water volume, temperature and time of synthesis (Scheme 2A and B). In general, all syntheses were accomplished as follows. The synthesized L-dopa DSDA was dissolved in degassed water. This mixture was heated (40–70°C) to achieve a homogeneous solution. Then, a co-structure directing agent (CSDA), APTES, was added to interact with the polar head of L-dopa DSDA to stabilise the micelles,[56] and the mixture gradually turned

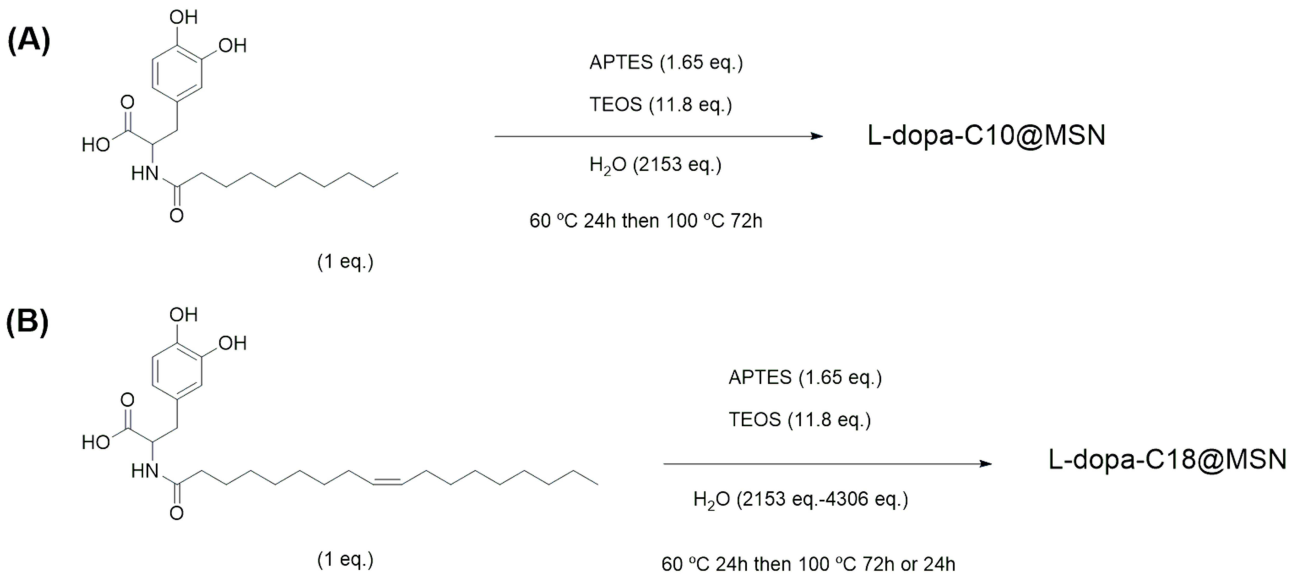

Scheme 2 Synthesis of L-dopa@MSNs.: (**A**) L-dopa-C10@MSN and (**B**) L-dopa-C18@MSN.

white. At this point, TEOS was added dropwise. The stirrer was removed from the reaction after 15 min. 24h later the synthesis was heated to 100°C for 24–72h. All synthetic conditions are summarize in Table 1:

PAMPA-BBB Assay

Prediction of the brain penetration was evaluated using the in vitro parallel artificial membrane permeability assay for the blood-brain barrier (PAMPA-BBB), as previously described.[57,58] This method is a useful high-throughput screening tool for the prediction of BBB permeability, but it is limited to the passive transport since lipid membrane used for the experiment cannot imitate active transport characteristics of endothelial cells. The acceptor 96-well microplate was filled with 200 µL of PBS: Ethanol (70:30) and the filter surface of the donor microplate was impregnated with 4 µL of PBL in dodecane (20 mg mL^{-1}). Compounds were dissolved in PBS:ethanol (70:30), filtered through a Millex filter, and then added to the donor wells (200 µL). The donor filter plate was carefully placed on the acceptor plate to form a sandwich, which was left undisturbed for 120 min at 25°C. After incubation, the donor plate was carefully removed and the compounds concentrations in the acceptor wells were determined using UV-Vis spectroscopy. Every sample was analyzed at five wavelengths, in four wells and at least in three independent runs, and the results are given as the mean ± SD. In each experiment, 10 quality control standards of known BBB permeability were included to validate and normalize the analysis set.

Table 1 L-dopa@MSNs Nanoparticles Synthetic Conditions

Nanomaterial	Synthesis Conditions (Temperature/Time)	DSDA:CSDA:TEOS:H_2O (eq.)
L-dopa-C18@MSN-1	60°C then 100°C 72 h	1:1.65:11.8:2153
L-dopa-C18@MSN-2	60°C then 100°C 24 h	1:1.65:11.8:2153
L-dopa-C18@MSN-3	60°C then 100°C 24 h	1:1.65:11.8:3229
L-dopa-C18@MSN-4	60°C then 100°C 24 h	1:1.65:11.8:4306
L-dopa-C18@MSN-5	70°C then 100°C 24h	1:1.65:11.8:3229
L-dopa-C18@MSN-6	40°C then 100°C 24h	1:1.65:11.8:3229
L-dopa-C10@MSN	60°C then 100°C 72 h	1:1.65:11.8:2153

Synthesis of MCM-41 Nanoparticles (Reference Material)

MSNs were synthesized following the next procedure:[59] CTAB (300 mg, 0.822 mmol) was dissolved in a mixture of 129.2 mL of milli-Q H2O and 18.5 mL of ethanol, with the subsequent addition of NaOH (1.55 mL, 1M) and the mixture was stirred at 82°C. Then, TEOS (1.55 mL, 6.95 mmol) was added dropwise to the solution, maintaining the stirring for 2 h. The final solid was isolated by filtration, washed three times with milliQ-H2O and EtOH and dried under vacuum. The surfactant was finally removed after calcination at 550°C for 5 h.

Incorporation of L-Dopa Onto the Surface of MCM-41 (L-dopa@MCM-41)

The functionalization of nanoparticles was carried out by adding 200 mg of material to a solution of L-dopa (50 mg, 0.25 mmol) in 50 mL of ethanol. Themixture was dispersed by sonication for 10 min at room temperature (37 KHz, 70% power) and then stirred at room temperature for 24 h. Thefinal solid was isolated by filtration, washed three times with milliQ-H_2O and EtOH and dried under vacuum. The amount of adsorbed L-dopa was determined by thermogravimetric analysis.

Release Experiments and in vitro Biodegradation Kinetics

The in vitro release studies of L-dopa were conducted under physiological conditions in PBS at pH 7.4, following the next procedure: L-dopa@MSNs (3 mg) were dispersed in 1 mL of PBS (pH 7.4) and hydrochloric acid-sodium chloride buffer (pH=1.2), and the dispersion was incubated at 37°C in a thermoblock at 900 rpm. The amount of L-dopa released was quantified by centrifuging the dispersion and subsequently measuring the absorbance at 280 nm of the supernatant using a spectrometer (Evolution 201 UV-Vis Spectrophotometer, ThermoScientific). After each measure, fresh PBS or hydrochloric acid-sodium chloride buffer was added.

The biodegradation kinetics in vitro were performed as follows: 5 mg of the material was suspended in 2 mL of FBS and the suspension was stirred at 37°C in a thermoblock at different times (0, 1, 3, 6 and 14 days). Aliquots were then centrifuged to separate the pellet from the supernatant. Pellets containing MSNs were analyzed by TEM.

Cell Culture

HEK-293 (human kidney cells, ATCC, Virginia, USA) were used in viability studies. The cell line was cultured in Dulbecco's modified Eagle's Medium (DMEM) supplemented with 10% fetal bovine serum and 1% penicillin-streptomycin. Cell cultures were maintained at 37°C in a humidified atmosphere containing 5% CO_2 and they were seeded at 30% confluence in DMEM in 12-well plates.

Cell Viability by MTT Assay

All cells were treated 48 h after being seeded with different concentrations of L-dopa, DSDA L-dopa-C18 and L-dopa-C18@MSN-3 and incubated for 48 and 96 hours. A pure MSN material MCM-41 type was also used as vehicle control.[59] The suspensions of L-dopa-C18@MSN-3 had been previously prepared by sonication of the nanoparticles in milliQ-H_2O for 10 min at 37°C to achieve complete dispersion. Then it was diluted with DMEM to achieve the desired concentration. After the treatment at different times, the cell viability was determined by the colorimetric assay MTT. This method relies on the capacity of viable cells to reduce MTT to formazan. The quantity of the reduction product is directly proportional to the viable cells, and it can be measured by the absorption of UV light. Thus, the MTT was added to cultured cells at a final concentration of 0.1 mg mL^{-1}. After 6h, the medium was removed, and cells were resuspended in DMSO and subsequently transferred to a 96-well plate. The absorbance was recorded at 542 nm in a spectrometer (Multiskan SkyHigh, ThermoScientific, URJC, Móstoles, Spain). Values are expressed as mean ± S.E.M. of at least three independent experiments.

Experimental Design

The antiparkinsonian effect of MSN containing L-dopa amide derivatives conjugated with fatty acids was evaluated in a unilateral intrastriatal 6-OHDA lesion model. Animals were randomly and blindly assigned into vehicle (VEH, sterile physiological saline) or treatment groups. Independent groups of animals were used for each treatment: saline, oleic acid

(C18), L-dopa, DSDA L-dopa-C18, L-dopa-C18@MSN-3 and L-dopa-C10@MSN. The dose of L-dopa was set at 25 mg kg^{-1} for all formulations based on previous work.[60,61] The human equivalent dose (HED) corresponding to 25 mg/kg in mice is approximately 2.02 mg/kg, which falls within the range of doses used in current clinical practice.[62] For oleic acid alone the dose was calculated based on the amount present in the MSN formulations. All drugs were administered intraperitoneally (i.p.) in a volume of 0.3 mL and their effect was tested 120 min to 14 days after single administration. Treated mice were compared with control (saline) and L-dopa treated groups. The effect of the treatment was also evaluated in healthy control naïve animals. All experiments were conducted on female mice, upon comparison of saline and L-dopa-C18@MSN-1 groups between male and female. A schematic depiction of the experimental design is provided in Figure 1.

6-OHDA Lesion

The unilateral 6-OHDA lesion in the striatum was performed as previously described[64] with minor modifications. Briefly, mice were analgesized (0.1 mg kg^{-1} buprenorphine, i.p)., anesthetized (0.75 mg kg^{-1} medetomidine, 7.5 mg kg^{-1} midazolam, i.p.) and infused with 20 μg of 6-OHDA in 2 μL sterile saline (10 μg μL^{-1}) delivered by a Hamilton syringe into the left striatum at the following coordinates from bregma: 0.5 mm anterior-posterior, - 2.0 mm lateral, - 3.0 mm dorsoventral, at a flow rate of 0.2 μL min^{-1}. At the end of the infusion, the syringe was left implanted for an additional 5 min per site and was then slowly retracted. During the surgery and recovery, animals were kept warm using a heating pad. 6-OHDA injections occurred 10 days prior to the initiation of any pharmacological administration. A group of control animals received 2 μL sterile saline (0.9% NaCl).

Behavioral Tests

In order to characterize the behaviors of intact or hemiparkinsonian mice, spontaneous rotation was assessed. Animals unable to reproduce the expected behavior were discarded.

Spontaneous Rotations

The spontaneous behavior of the animals was analyzed using a video camera as previously described.[65] Contraversive and ipsiversive rotations were evaluated in a test cage every other day from day 0 to day 13, and on days 20 and 24. Additionally, further evaluations were performed between days −4 and −1. Each data set consisted of a 15 min test period. Although the test is based on the assumption that mice turn towards the lesioned side when placed in a novel environment,[66] there may be an endogenous asymmetry in the nigrostriatal dopaminergic system, eg regarding the dominant side. Consequently, the preferred direction of rotation may vary between individuals over time, regardless of whether the depletion is always performed on the same side.[67] Therefore, the number of complete 360° rotations made in both the ipsiversive and contraversive directions relative to the lesion was counted. Based on the assumption that the greater the bias towards one side, the more parkinsonian the animal, rotational behavior was expressed as the proportion of ipsiversive (alternatively contraversive if greater) rotations over total rotations (contraversive and ipsiversive) normalized to the pre-parkinsonian phase (mean value for days [−4 to −1]). To avoid the possibility of data bias due to unreliable/inconsistent lesions, animals unable to perform ≥ 15 rotations during 15 min on any day of the parkinsonian phase (days 0 to 10) were subject to discard.[68,69]

Body Weight

Body weight was periodically recorded as an indirect measure of animal welfare in order to assess actual severity at the end of the procedure, as collected under Directive 2010/63/EU on the protection of animals used for scientific purposes (European Commission, 2019).

Statistical Analysis

All data were analyzed and plotted on graphs using the GraphPad Prism 8.0 software. In cell viability studies, two-way ANOVA (treatment x concentration), followed by Tukey's multiple comparisons test was used to analyze the difference between the means of treatment and control groups over time. Values of $P < 0.05$ were considered statistically significant.

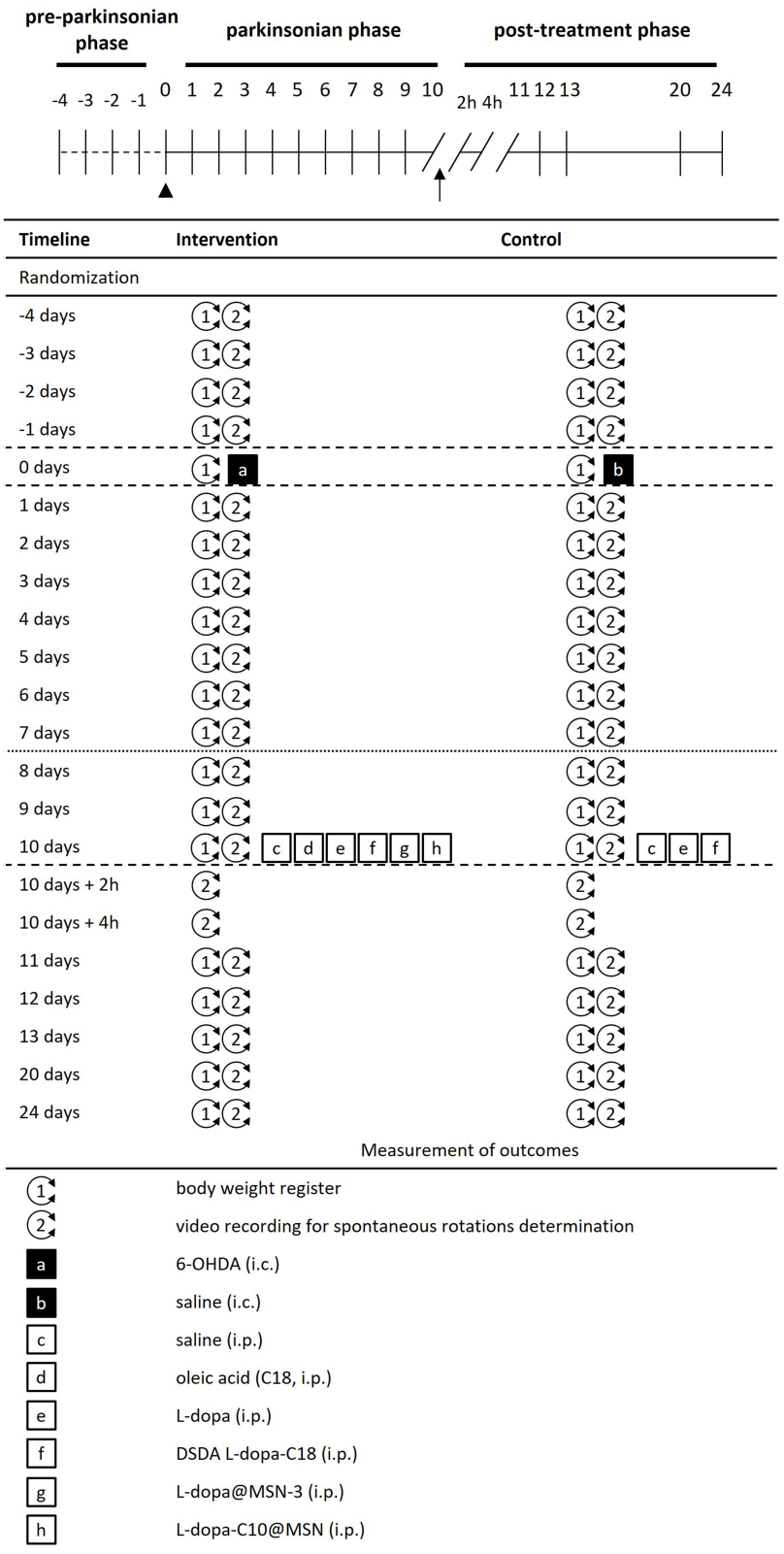

Figure 1 Graphical depiction of the complex intervention delivered over a 30-day period (adapted from Ayieko et al).[63] The intervention components are labeled 1–2 and a–h. Circles represent behavioral tests and squares represent interventions; one treatment per experimental group. Arrowhead and black squares indicate 6-OHDA or saline i.c. administration. Arrow and white squares, the i.p. administration of the different experimental formulations.

https://doi.org/10.2147/IJN.S545116

T-test was used to compare cell viability results at 48h and 96h. In animal studies, the normality of all data was assessed by the Shapiro–Wilk test. Two-tailed paired *t*-test or alternatively Mann–Whitney *U*-test (non-normal distribution) were used to compare the outcomes (spontaneous rotational behavior) of sham control and 6-OHDA groups and between female and male mice. One-way ANOVA followed by Dunnett's multiple comparisons test was used to assess differences between treatments in sham saline-treated (i.c.) animals. For all treatment groups, one-way ANOVA within-group comparisons followed by Dunnett's multiple comparisons test were also made against their corresponding mean values obtained on day 10. Two-way ANOVA (treatment x time), followed by Tukey's multiple comparisons test was used to analyze the difference between the means of treatment and control groups over time. Values of $P < 0.05$ were considered statistically significant.

Results and Discussion

Synthesis and Characterization of MSNs with L-Dopa-C18 DSDA

The initial phase of this study is concerned with the synthesis conditions of MSNs containing L-dopa derivatives as a surfactant, with the objective of maximizing the amount of L-dopa loaded into mesoporous silica nanoparticles (MSNs) and optimizing their size for further use in the in vivo behavioral assessment. Water volume, synthesis temperature and time were studied as variables to obtain MSNs. The first step involved the synthesis of DSDA based on L-dopa. The anionic DSDA of L-dopa was successfully achieved through the amidation reaction between the amino group of the L-dopa and two different acyl chlorides, decanoyl chloride and oleoyl chloride (Scheme 1). The DSDAs exhibited amphiphilic characteristics, comprising a polar head and an aliphatic chain that enabled their use as a templates for the synthesis of MSNs.[52] The successful formation of the amide bond was confirmed by ^{1}H, ^{13}C NMR, MS, FTIR spectroscopy and EA (Figures S1–S7 and Table S1).

The potential passive diffusion in the central nervous system (CNS) of the DSDAs L-dopa-C10 and L-dopa-C18 was evaluated through a PAMPA assay. As illustrated in Table S2, the DSDA L-dopa-C18 exhibited a higher permeability (Pe = 1.13 cm s^{-1}) than its precursor L-dopa (Pe = 0.94 cm s^{-1}). Although the calculated permeability coefficient classified the L-dopa-C18 compound as CNS-, indicating low blood-brain barrier (BBB) penetration, it is well established that L-dopa utilizes an amino acid transporter to traverse the BBB (L-type amino acid transporter-1, LAT-1).[70] Previous reports indicate that LAT-1 interacts with various amino acid-derived prodrugs (including prodrugs synthesized from dopamine), thereby improving their brain uptake.[71,72] Additionally, the hydrophobic oleic acid tail might facilitate transient interactions with lipid components of the BBB, enhancing transport efficiency. This, in conjunction with the enhanced permeability observed for L-dopa-C18 relative to L-dopa, would suggest an enhancement in passive diffusion to cross the BBB for this DSDA.[73,74] Furthermore, previous in vitro research[49] has demonstrated that DSDAs can be cleaved by the enzyme chymotrypsin, suggesting that they may also be released as L-dopa and oleic acid, which would indicate that both compounds can be found in their original therapeutic form. Consistent with this, an amide L-dopa prodrug administered to rats exhibited low plasma levels, likely due to rapid enzymatic conversion to L-dopa.[75]

Using both DSDAs, it has been achieved MSNs with a high surface area and significantly higher amounts of encapsulated L-dopa compared to traditional methods.[46] This L-dopa@MSNs have been characterized by TEM, DLS measurements, BET analysis and TGA analysis (Figures S8–10). An optimization process was carried out using DSDA L-dopa-C18. As mentioned before, the synthesis parameters examined were water volume, synthesis temperature and time. A complete description of synthetic conditions used can be found in Table 1.

The first parameter to be evaluated was the synthesis time. L-dopa-C18@MSN-2 was obtained by reducing the synthesis time from 72 to 24 h. Reducing the synthesis time from 72 to 24 hours clearly influences the size of the nanoparticles obtained, as shown in Figure 2A and B. The significant reduction in particle size led to setting the synthesis time at 24 hours for the rest of the syntheses evaluated. Next, the effect of the DSDA:H_2O ratio on the size and morphology of the nanoparticles was evaluated. High dilutions keep the nuclei of the primary particles separate, so increasing the water volume of the synthesis has been used before as a strategy to reduce nanoparticle size.[76] This strategy allows us to reduce the nanoparticle size down to 140 nm in the case of L-dopa-C18@MSN-3 (Figure 2C) and 74 nm in the case of L-dopa-C18@MSN-4 (Figure 2D). Regarding the nanoparticles shape, L-dopa-C18@MSN-3 mainly shows monodisperse spherical

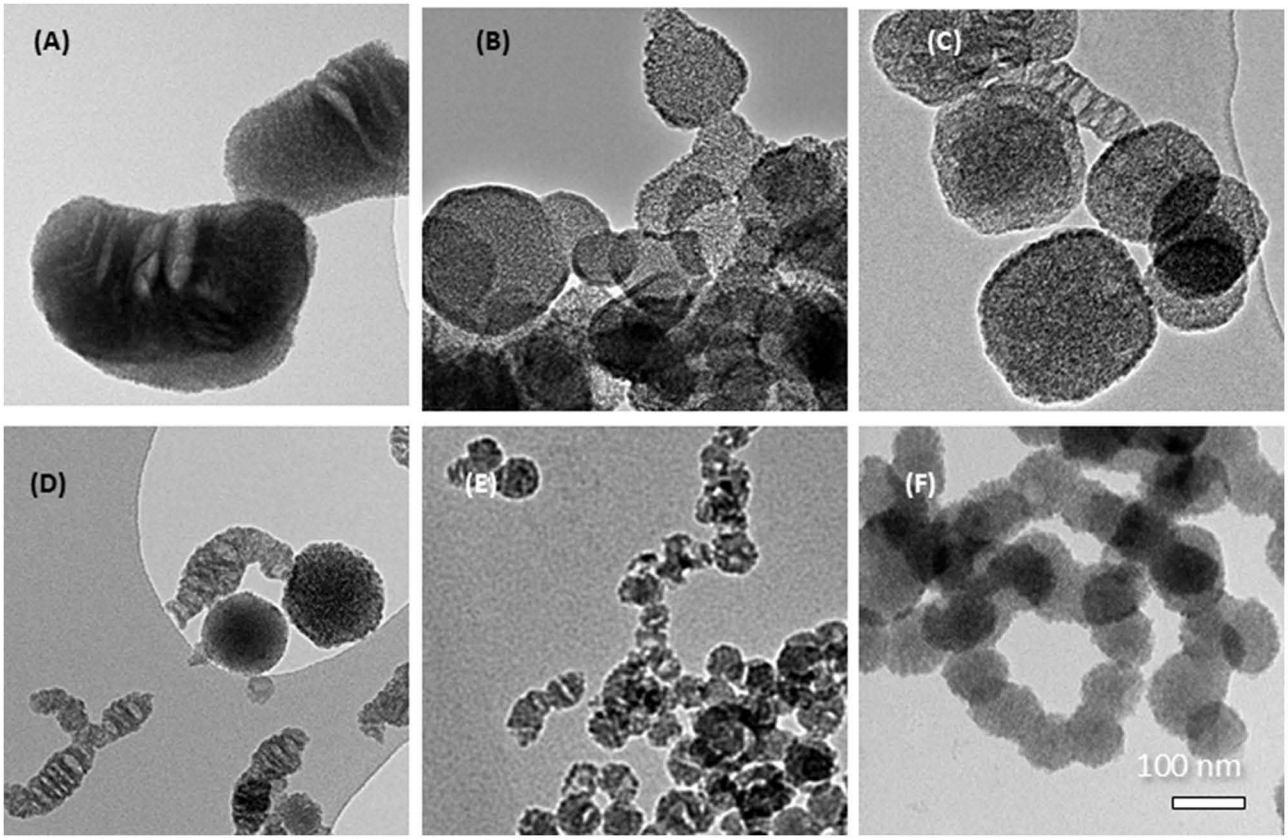

Figure 2 TEM images obtained from synthesis variation: (**A**) L-dopa-C18@MSN-1; (**B**) L-dopa-C18@MSN-2; (**C**) L-dopa-C18@MSN-3; (**D**) L-dopa-C18@MSN-4; (**E**) L-dopa-C18@MSN-5; (**F**) L-dopa-C18@MSN-6. Scale bar 100 nm.

nanoparticles, meanwhile, L-dopa-C18@MSN-4 predominantly exhibits hollow elongated structures (Figure S8D). Finally, an evaluation of the impact of different temperatures on the synthesis process was conducted. The synthesis conducted at 70°C (L-dopa-C18@MSN-5) yielded nanoparticles with a diameter below 60 nm, as illustrated in Figure 2E. This increase in temperature resulted in the formation of inter-nanoparticle necks, leading to the development of elongated hollow-shell structures. The synthesis performed at 40°C (L-dopa-C18@MSN-6) resulted in the formation of small nuclei that were aggregated among themselves (Figure 2F). The TEM and DLS measurements confirmed that L-dopa-C18@MSN-5 and L-dopa-C18@MSN-6 exhibited a high degree of aggregation (Figure S8E and F).

The textural properties of the synthesized materials (Table 2) were determined from the isothermal nitrogen adsorption experiments, with BET surface area values ranging from 300 and 700 $m^2\ g^{-1}$ and pore sizes between 2.5 and 4.2 nm. A type IV isotherm, according to IUPAC classification, was obtained for all MSNs (Figure S9), which is

Table 2 Textural Properties of MSNs Obtained from Synthetic Optimization

Nanomaterial	BET Surface ($m^2\ g^{-1}$)	Vp ($cm^3\ g^{-1}$)	Dp (nm)
L-dopa-C18@MSN-1	556	0.52	3.2–3.7
L-dopa-C18@MSN-2	303	0.33	3.7
L-dopa-C18@MSN-3	509	0.69	3.9
L-dopa-C18@MSN-4	693	0.82	3.3–4.2
L-dopa-C18@MSN-5	621	0.87	3-4.3
L-dopa-C18@MSN-6	423	0.54	3.6
L-dopa-C10@MSN	360	0.21	2.5

https://doi.org/10.2147/IJN.S545116

characteristic of MCM-41-type materials. A hysteresis loop was observed at 0.4 p/p_0. All synthesized samples exhibited a narrow pore distribution (Figure S9). L-dopa-C18@MSN-4 and MSN-5 displayed bimodal and even trimodal PSD, which can be attributed to the inter-particular necks previously mentioned. The observed similarity in pore distributions can be attributed to the use of the same DSDA in the synthesis of MSN. The sample synthesized from the DSDA L-dopa-C10 shows the smallest pore size (Table 2). As is well known, pore diameter (Dp) varies with the length of aliphatic chain of surfactant.[52] All the isotherms (with the exception of L-dopa-C18@MSN-1, −2 and −3) exhibit a second hysteresis loop at higher relative pressure (approximately at 0.9 p/p_0), which can be attributed to inter-particle porosity[77] (Figure S9).

Based on the previous results, two materials were considered for their optimal physico-chemical properties, L-dopa-C18@MSN-1 and L-dopa-C18@MSN-3. The morphology, size, and textural properties of L-dopa-C18@MSN-1 and L-dopa-C18@MSN-3, together with their L-dopa content, are illustrated in Figure 3. These materials exhibit different morphology and an increment in the quantity of L-dopa loaded. The morphology and size of these MSNs were determined using TEM images. The L-dopa-C18@MSN-1 sample (Figure 3A and B), obtained under initial synthetic conditions[52] (Table 2), showed different type of nanoparticles in size and shape. While some of the nanoparticles presented spherical symmetry with sizes between 200–400 nm, others displayed an elongated hollow-shell structure with a length range from 300 to 600 nm (Figure 3A and B, Figure S8A). TEM images obtained for the sample L-dopa-C18 @MSN-3 (Figure 3C and D, Figure S8C) revealed the presence of spherical and monodisperse nanoparticles with an average diameter of 140±40 nm. These differences were confirmed by DLS measurements. The distribution function obtained for sample L-dopa-C18@MSN-3 (Figure 3F) is narrower than the distribution function of L-dopa-C18@MSN-1 (Figure 3E). Previous studies have indicated that the optimal nanoparticle size range for achieving long-term circulation of a DDS is between 10 and 200 nm. Nanoparticles below 10 nm in size may be rapidly excreted by the kidneys, whereas those above 200 nm may activate the macrophage system and be rapidly removed from the bloodstream.[38,40] A comparison of the results obtained by TEM and DLS suggests that the L-dopa-C18@MSN-3 sample may have been more suitable for prolonged circulation within the organism. Based on the previous results, we selected the L-dopa-C18@MSN-3 for the subsequent evaluation in vivo tests. In addition, the L-dopa-C10@MSN was also selected to study the influence of the alkyl chain.

Figure 3G and H shows SEM images of samples L-dopa-C18@MSN-1 and MSN-3. The micrographs display a textured and rough surface covered with small protrusions. Additionally, the SEM image of L-dopa-C18@MSN-1 (Figure 3G) reveals the presence of an inner cavity within a crushed nanoparticle, which aligns with the observations made in the TEM and the presence of internal voids. Furthermore, FTIR analysis was conducted to confirm the incorporation of the drug. The spectrum showed a band from 1750 cm^{-1} to 1600 cm^{-1}, indicative of the stretching vibration of amide of DSDA, along with a prominent peak at 2900 cm^{-1}, which can be attributed to the presence of multiple C-H bonds from the tail of DSDA. The FTIR spectrum of the MSNs exhibited the characteristic bands associated with the formation of the silica framework, including a strong band at 1100 cm^{-1} assigned to the asymmetric stretching of the -Si-O-Si- and a symmetric stretching band at 760 cm^{-1} (Figure 3I). Additionally, the quantity of organic material present was determined by TGA (Figure S10). The organic content of L-dopa-C18@MSN-1 was determined to be 29%, while that of the L-dopa@MSN-3 was found to be 63% (Figure 3J). This thermal decomposition corresponds to both DSDA and CSDA. The content of L-dopa loaded in the MSNs was determined through TGA of calcinated and extracted samples (Figure S11). From these data, it can be inferred that 8% of the weight of L-dopa-C18@MSN-1 sample corresponds to L-dopa, meanwhile the amount of L-dopa loaded in L-dopa-C18@MSN-3 was 22%. The different amount of L-dopa loaded between these materials contrasts with their similar surface area, 556 and 509 $m^2\ g^{-1}$ for L-dopa-C18 @MSN-1 and MSN-3, respectively (Figure 3K). A kinetic explanation for the synthesis formation could account for these differences. By reducing the synthesis time and increasing the dilution in water, it appears that the nanoparticles lack the capacity to aggregate, and form elongated nanoparticles with internal voids, from which the DSDA is excluded (L-dopa-C18@MSN-1). In contrast, the more solid but porous nanoparticles in the case of L-dopa-C18@MSN-3 have a higher L-dopa loading capacity. Finally, to determine the distribution of the drug within the MSNs, EDS mapping analysis was performed for L-dopa@MSN-3 sample. The resulting images show a homogeneous distribution of silicon, carbon, oxygen and nitrogen on the surface of the MSN (Figure 3L-O).

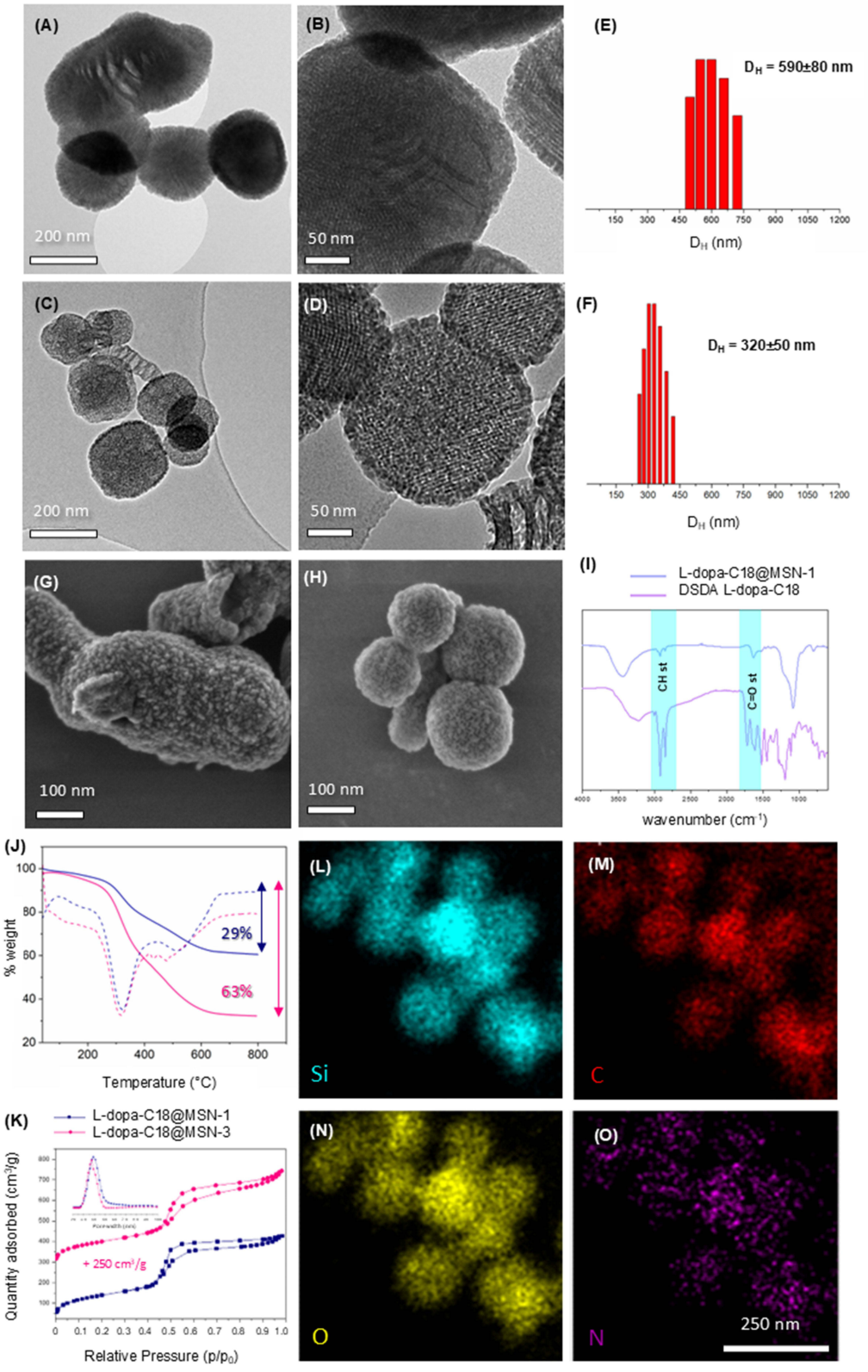

Figure 3 TEM images for (**A** and **B**) L-dopa-C18@MSN-1 and (**C** and **D**) L-dopa-C18@MSN-3. Hydrodynamic diameter measured by DLS for (**E**) MSN-1 and (**F**) MSN-3. SEM images of (**G**) MSN-1 and (**H**) MSN-3. (**I**) N_2 adsorption isotherms of L-dopa@MSN-1 in blue and L-dopa@MSN-3 in red. (**J**) FTIR spectrum of L-dopa DSDA and L-dopa MSN (**K**) TGA of L-dopa-C18@MSN-1 (in blue) and L-dopa-C18@MSN-3 (in pink). EDS mapping analysis: (L) Silicon, (M) carbon, (N) oxygen and (O) nitrogen distribution in MSN-3.

https://doi.org/10.2147/IJN.S545116

Release Experiments, Biodegradation and Biocompatibility

Once the successful incorporation of the drug was confirmed, the mechanism of drug release was investigated. In vitro release studies were carried out at in PBS buffer at physiological pH of 7.4 for L-dopa-C18@MSN-3 material. As illustrated in Figure 4A the release profile at pH=7.4 demonstrates a continuous increase in the amount of L-dopa over time, with the release of L-dopa continuing to rise beyond 14 days, as yet not reaching a plateau. Interestingly, at pH=1.2 (simulated gastric fluid), L-dopa decreased when compared to pH=7.4, likely due to carboxylic acid protonation, which makes the DSDA much less soluble than at pH=7.4. This pH-responsive behavior suggests that L-dopa-C18@MSN-3 could be promising for oral administration, enabling release in the intestine, the primary absorption site for L-dopa. The release kinetics of L-dopa-C18@MSN-3 differ markedly from those of conventional drug-loaded mesoporous silica nanoparticles (MSNs), in which the drug is adsorbed onto the surface or mainly

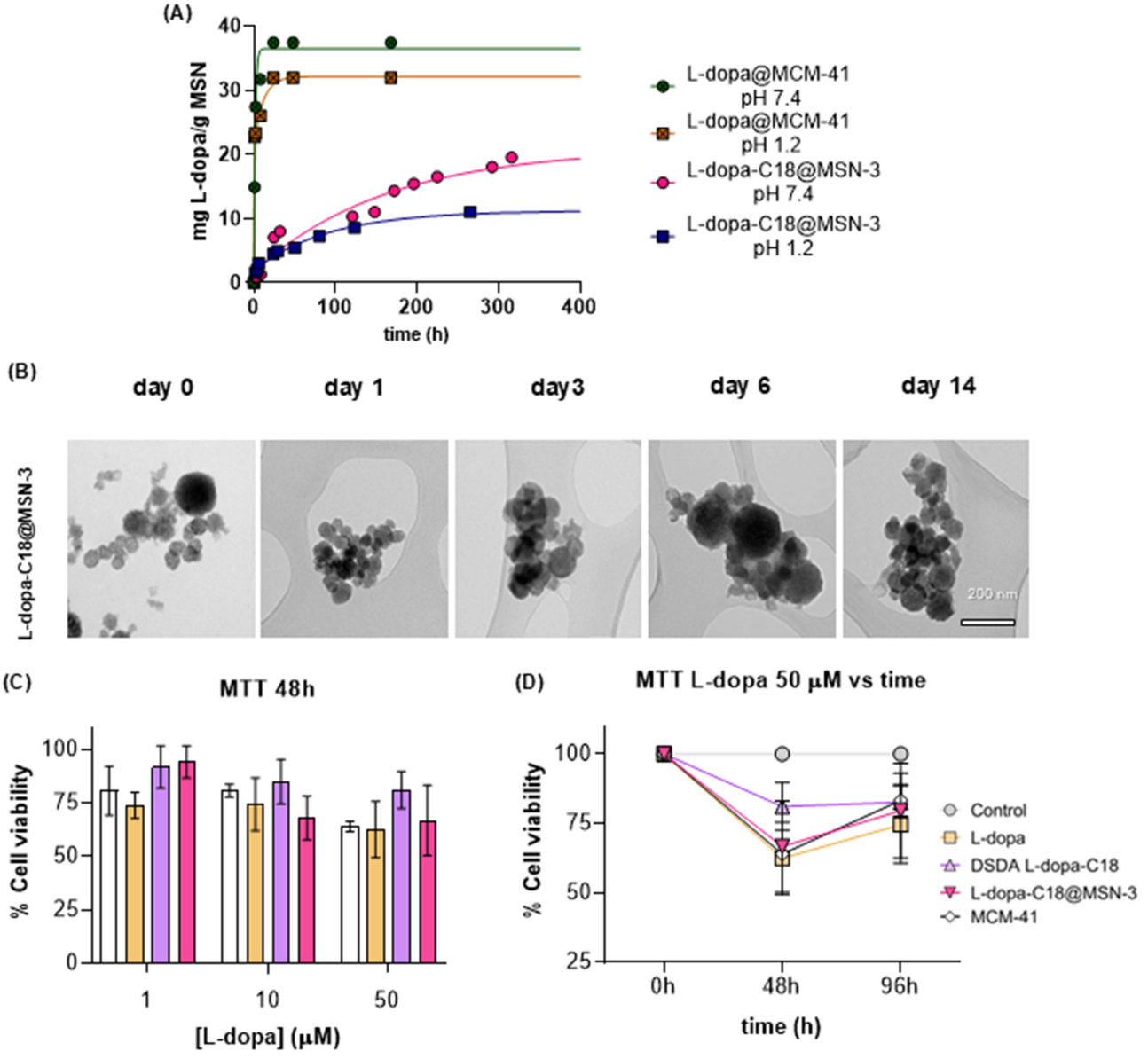

Figure 4 (**A**) L-dopa release study from L-dopa-C18@MSN-3 represented as mg L-dopa/g material at pH = 7.4 and at pH 1.2. Release study of the L-dopa loaded through adsorption in a reference material (MCM-41). (B) TEM images of biodegradation of L-dopa-C18@MSN-3 study at 0, 1, 3, 6 and 14 days. (C) Cell viability of free L-dopa, DSDA L-dopa-C18 and L-dopa-C18@MSN-3 in HEK-293 at 48 h. (D) Cell viability curves corresponding to the treatment at 48 and 96 h HEK-293 cells with free L-dopa (yellow), DSDA L-dopa-C18 (purple) and L-dopa-C18@MSN-3 (pink). MCM-41 (white) was used to evaluate MSNs cytotoxicity. Values are expressed as mean ± S.E.M. of at least three independent experiments.

within the pores. In the case of conventional adsorbed L-dopa on MSN, L-dopa@MCM-41 (Figure 4A), a premature release was observed, with up to 38 and 32 mg/g of L-dopa released (76% and 65% of total content) within 24 hours at physiological and acidic pH, respectively (pH 7.4 and pH 1.2). These results are consistent with previous studies showing that most of the L-dopa in conventionally loaded MSNs is released within a short time frame.[46] This rapid release is attributed to the immediate solvent exposure of the adsorbed drug, which is typical of conventional MSNs where mesopores remain partially unoccupied. In contrast, in L-dopa-C18@MSNs, the prodrug is densely packed within the mesopores, allowing only the fraction located at the outer surface to interact with the surrounding medium. Moreover, the higher hydrophobicity of the L-dopa-C18-based DSDA likely contributes to the markedly slower release observed for this formulation.[53] Therefore, L-dopa-C18@MSNs provide a sustained release profile, potentially maintaining therapeutic plasma concentrations longer than free L-dopa, leading to a steady influx into the brain. L-dopa DSDA-synthesized MSNs maximize material porosity while preventing premature drug release common with traditional loading methods.[50–53] Additionally, encapsulation may shield L-dopa from peripheral metabolism, increasing the amount available for BBB transport.[53,78]

In addition, biodegradation studies in simulated body fluid (FBS) environment were performed, wherein alterations in the morphology of MSN were examined using TEM. Figure 4B displays the degradation process of L-dopa-C18@MSN-3. TEM images show a gradual merging of nanoparticles. By day 6, the boundaries in the MSNs become indistinct. These results unequivocally demonstrate the degradation of MSNs in simulated body fluid, indicating the biocompatibility of the material for use as a DDS. The safety and biocompatibility of MSNs have been extensively demonstrated in several studies, with no toxicity concerns associated with their used as nanovehicles.[26]

To assess the safety profile of these L-dopa@MSNs, cell viability tests were performed in vitro, evaluating their toxicity in healthy kidney cells (HEK-293) at different concentrations after 48 h. To carry out these experiments, free L-dopa and the DSDA were used as controls and calcined MCM-41 material as reference to evaluate MSNs toxicity. As shown in Figure 4C, following a 48-hour incubation period, the administration of L-dopa-C18@MSN-3 at a concentration of 1 μM exhibited minimal adverse effects on cell viability, with only 5% of cell death, comparable to that observed with DSDA. In contrast, the free L-dopa reduced cell viability by 25%. The increase in doses to 10 and 50 μM did not produce statistically significant differences compared to those obtained with 1 μM. There is only a decline in the case of the nanoparticles (MCM-41 and L-dopa-C18@MSN-3), which may be attributed to the high amount of material required to achieve the desired concentration of the L-dopa derivative and not to the direct effect of this compound on the cells. One way and two-way ANOVA were performed to analyze the effect of concentration and treatments respectively on cell viability. No statistically significant differences were observed at 48h.

With these good results, we decided to perform a second experiment increasing the incubation time until 96 h at the maximum concentration, testing if cells could show a recovery in the presence of the selected drugs. As illustrated in Figure 4D, cells treated with both L-dopa-C18@MSN-3 and the free L-dopa exhibited a clear and similar recovery (approximately 15%) in their population after 96 h, indicating that the release of the L-dopa derivative from the nanoparticles does not induce toxic effects on cells. In the literature, L-dopa has been described as cytotoxic, potentially due to autoxidation and subsequent formation of the o-quinone derivative.[79,80] However, the encapsulation of the drugs in the nanoparticles can be an effective technique to reduce associated toxicity issues. On the other hand, cells treated with the DSDA did not exhibit increased mortality after 96 h, indicating that this molecule does not produce toxic effects over longer times. A *t*-test was performed to compare cell viability at 48h and 96h. No statistically significant differences were observed among 48h and 96h.

By optimizing the synthesis procedure, it has been possible to maximize the amount of L-dopa loaded into the MSNs. The results of in vitro assays reveal pH-responsive behavior and a sustained over time for L-dopa-C18@MSN-3. Moreover, cell viability assays show that the L-dopa@MSN does not induce toxic effects, thereby indicating that L-dopa-C18@MSN-3 could be the optimal nanoformulation to be used in the in vivo test.

 https://doi.org/10.2147/IJN.S545116

Behavioral Assessment

Evaluation of L-dopa@MSNs vs Free-L-Dopa Administration in the Spontaneous Rotational Behavior Performed by the Animals

Whilst most of the literature focuses on the immediate effects, the long-term behavioral consequences of the unilateral 6-OHDA model have been sparsely documented in both rats[81] and mice.[82] Furthermore, there are discrepancies in the methodology employed across studies, with variations in the injection site, dose, unilateral/bilateral nature of the lesion, and animal sex and strains. As a result, precedent evidence is often not a suitable basis for comparison in many cases. Unlike other models like neurotoxin 1-methyl-4-phenyl-1,2,3,6-tetrahydropyridine (MPTP) lesions, 6-OHDA would yield both partial and complete destruction of dopaminergic cells at the injected area with no spontaneous recovery, accounting for long-lasting reduction in the dopamine content within the striatum with the underlying behavioral deficits.[83] In the present study, unilateral intracranial injection of 20µg 6-OHDA in the dorsal striatum was performed in CD-1 mice, as previously described.[64]

Unilateral 6-OHDA injection in the striatum (caudate-putamen) evoked the classic parkinsonian response, manifesting as an increased frequency of spontaneous rotations that subsequently exhibited a tendency towards stabilization over time. After assessing normal distribution of data by Shapiro–Wilk test, a Mann–Whitney *U*-test was performed to compare the percentage variation in spontaneous rotational behavior between the vehicle saline (sham) and 6-OHDA groups. A significant difference was observed; U = 36, P < 0.001 (Figure 5). No statistically significant differences were observed between female and male mice; U = 144, P > 0.999 (Figure S12A).

Although spontaneous circling diminishes after the lesion, previous studies have reported a degeneration of nigrostriatal neurons and other locations over a period of 4–8 weeks, with a peak loss of neuron numbers occurring after 2–3 weeks, depending on the concentration of 6-OHDA used,[84] which is consistent with the stabilization we could observe after 10 days. 6-OHDA dose was chosen bearing in mind that the stereotyped behavior is stronger in animals with larger lesions.[85] Additionally, the use of amphetamine or apomorphine to induce a burst of turnings was not considered, as the objective was to evaluate the long-term efficacy of the treatment. Repeated administration of the trigger could lead to misleading conclusions. The majority of animals exhibited a rotational behavior similar to that previously described.[68,69,84,86] In some cases, the spontaneous rotations exhibited by the animals involved a circular

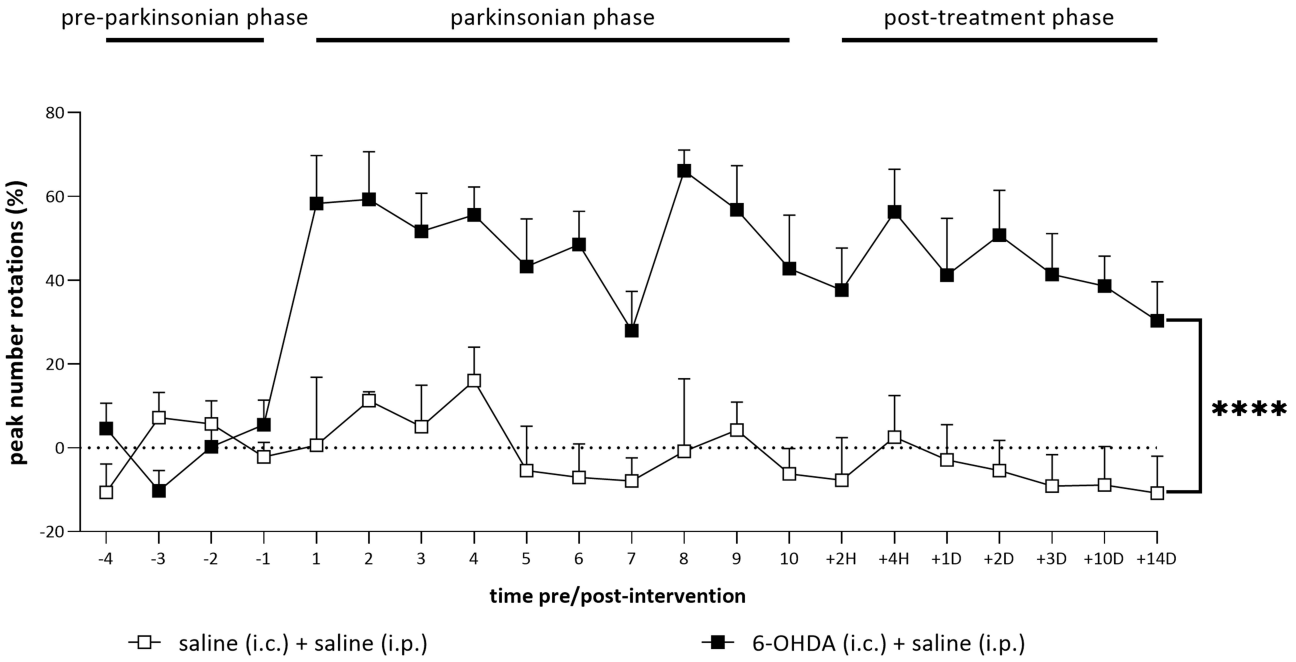

Figure 5 Time course of sham-injected control and 6-OHDA-induced parkinsonian behavior in mice treated with saline (i.p.) on day 10. Data are reported as mean percent of total rotations made in the contraversive or ipsiversive direction in 15 min normalized to [D-4–D-1] ± S.E.M. **** P < 0.001, Mann–Whitney *U*-test. N = 7–8 per group.

motion around the cage rather than a spinning motion. Nevertheless, all the animals displayed this repetitive behavior in a uniform manner. A non-negligible number of animals started to perform or exhibited a contraversive net score from the moment 6-OHDA was administered. A preferential rotational side was also observed on some days for some animals between days 4 and 1 prior to 6-OHDA, and in some animals receiving an injection of innocuous sterile physiological saline. The number of animals is far too large to attribute this variability to manual bias in 6-OHDA injection or rotation test analysis. Interestingly, this has only been addressed once before.[67] The authors suggested that in some animals there may be an endogenous asymmetry in the nigrostriatal dopaminergic system with respect to the dominant side. Consequently, the preferred direction of rotation may vary over time between individuals, regardless of whether the depletion is always performed on the same side. Additionally, some authors have previously suggested that the rotation test may be a poor predictor of the 6-OHDA-lesion success[87] and outcome analysis is highly heterogeneous among studies (eg, contraversive rotations,[22,88–90] net ipsiversive rotations,[65,66,84,87] net contralateral rotations,[66,91] overall rotational behavior).[68] Therefore, we used the proportion of the peak number rotations (ipsiversive or contraversive, as may correspond for each timepoint) over total rotations normalized to those obtained for the pre-parkinsonian phase (D-4 to D-1) to reduce the bias from variations over time and between individuals.

A two-way ANOVA followed by Tukey's multiple comparisons test was performed to compare the percentage variation of the spontaneous rotational behavior between i.p. saline and treatment groups in i.c. saline and 6-OHDA injected animals over time. All 6-OHDA lesioned animals shared similar values on day 10 prior to i.p. saline or treatment and no statistically significant differences were observed against 6-OHDA control (Figure 6). Differences between sham and 6-OHDA control groups were evident at both 4-hour ($P < 0.05$, +2H and +4H) and 14-day follow-up ($P < 0.01$ for +2D, +3D and +10D, $P < 0.05$ for +14D). Despite all treatments showed reduced spontaneous rotational behavior at all timepoints compared to 6-OHDA control, statistically significant differences were only observed for L-dopa at +4H ($P < 0.05$), DSDA L-dopa-C18 at +10D and L-dopa-C18@MSN-3 at +2D and +10D. That is, L-dopa administration induced an acute effect and L-dopa-C18@MSN-3 outlasted free L-dopa. To further illustrate the efficacy of the L-dopa-C18@MSN-3 formulation, two videos provided in Additional File demonstrate the behavioral differences between untreated parkinsonian mice and those treated with the novel L-dopa-C18@MSN-3 formulation (Supporting Information, SI video-1 and −2). The first video shows the characteristic ipsiversive compulsive rotations of untreated parkinsonian mice, while the second video highlights the normalized behavior observed in animals following treatment with L-dopa-C18@MSN-3. This visual evidence reinforces the significant therapeutic potential of the new formulation in mitigating motor dysfunction associated with Parkinson's disease. C18 free and L-dopa-C10@MSN had no effect at all. This is further corroborated by the fact that 6-OHDA control and C18 showed statistically significant differences against sham control from the second day onwards ($P < 0.05$ for +2D, +3D and +14D) and also did L-dopa after 3 days ($P < 0.05$ for +3D and +14D), but not L-dopa-C18@MSN-3. However, when one-way ANOVA within-group comparisons followed by Dunnett's post-hoc test were made between post-treatment timepoints and their corresponding mean values obtained on day 10, no statistically significant differences were seen for any group. This may indicate that dose quantity and the single dose used to achieve the expected efficacy fell short.

No statistically significant differences were observed between female and male mice receiving L-dopa-C18@MSN-1; two-tail paired *t*-test, $t(16) = [1.318]$, $P = 0.206$ (Figure S12B). No statistically significant differences were either seen among treatments in sham saline-treated mice; one-way ANOVA followed by Dunnett's multiple comparisons test, $F(2.456, 38.480) = [2.630]$, $P = 0.074$ (Figure S13).

Assessment of Actual Severity at the End of the Procedure

Neither the intracranial saline nor the 20 µg 6-OHDA lesion groups substantially affected the mice body weight. Despite an initial weight loss (≤10%) after i.c. saline injection, control sham naïve mice experienced an overall progressive weight gain until sacrifice (Figure 7A). Similar trends were observed in animals receiving 6-OHDA (i.c.) over time (Figure 7B).

Despite the widespread use of the unilateral 6-OHDA lesion model in mice, longitudinal assessment of motor function in the literature is scarce and hence studies that report the long-term follow-up efficacy of treatments too. A limitation may lay on the fact that most studies rely on amphetamine or apomorphine as motion triggers, but this limits the follow-up of the impact of any experimental treatment. Repeated administration may distort the analysis of the effect

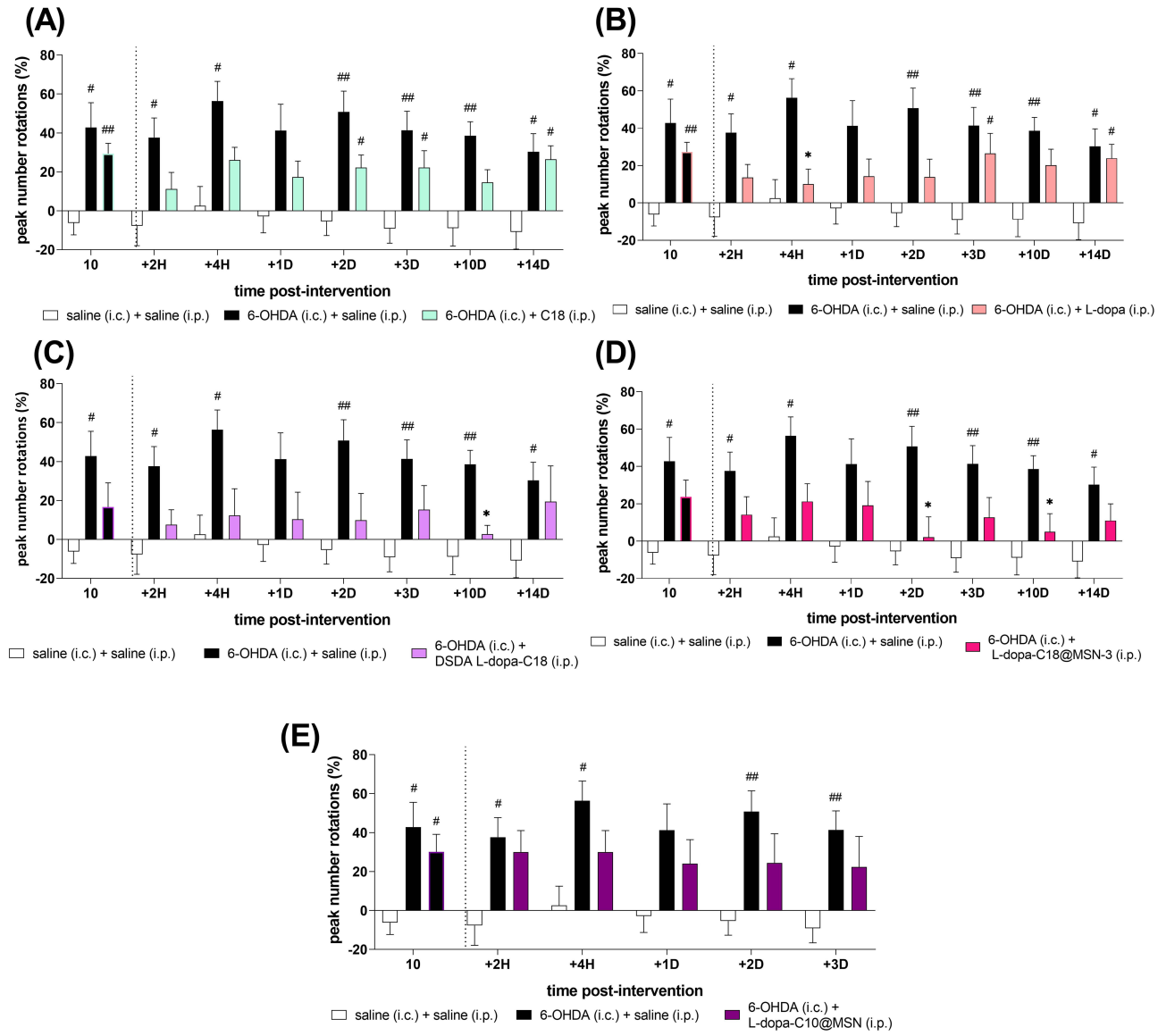

Figure 6 14-day follow-up comparison of the spontaneous rotational behavior exhibited by the different groups following intraperitoneal drug administration: (**A**) 6-OHDA +C18, (**B**) 6-OHDA+L-dopa, (**C**) 6-OHDA+DSDA L-dopa-C18, (**D**) 6-OHDA+L-dopa-C18@MSN-3 and (**E**) 6-OHDA+L-dopa-C10@MSN Data are expressed as peak number rotations over total number of rotations (ipsiversive and contraversive) relative to the mean value obtained for the pre-parkinsonian phase (%). *P < 0.05 vs 6-OHDA (saline, i.p).; $^{\#}$P < 0.05 and $^{\#\#}$P < 0.01 vs sham control (saline, i.p). Two-way ANOVA followed by Tukey's multiple comparisons test. N = 6–12 per group.

of the experimental drug. On the other hand, the rotational behavior in animals not subjected to amphetamine or apomorphine is not that impressive, so few articles have evaluated spontaneous rotations. Despite the low dose of L-dopa used herein, whether administered as free-L-dopa or encapsulated as L-dopa-C18@MSN-3, the observed trend suggests the potential therapeutic value of the novel experimental formulation. While the dose may have been insufficient to achieve better statistically significant differences, the results provide promising preliminary evidence supporting the efficacy of this approach. This work represents a compelling pilot study, laying the groundwork for further research to optimize dosing and to evaluate the full therapeutic potential of MSN-based L-dopa delivery systems.

Conclusion

The aim of this study was to engineer mesoporous silica nanoparticles (MSNs) using L-dopa amide derivatives (the DSDA approach) to maximize drug loading, minimize premature release and enhance functional outcomes in a mouse

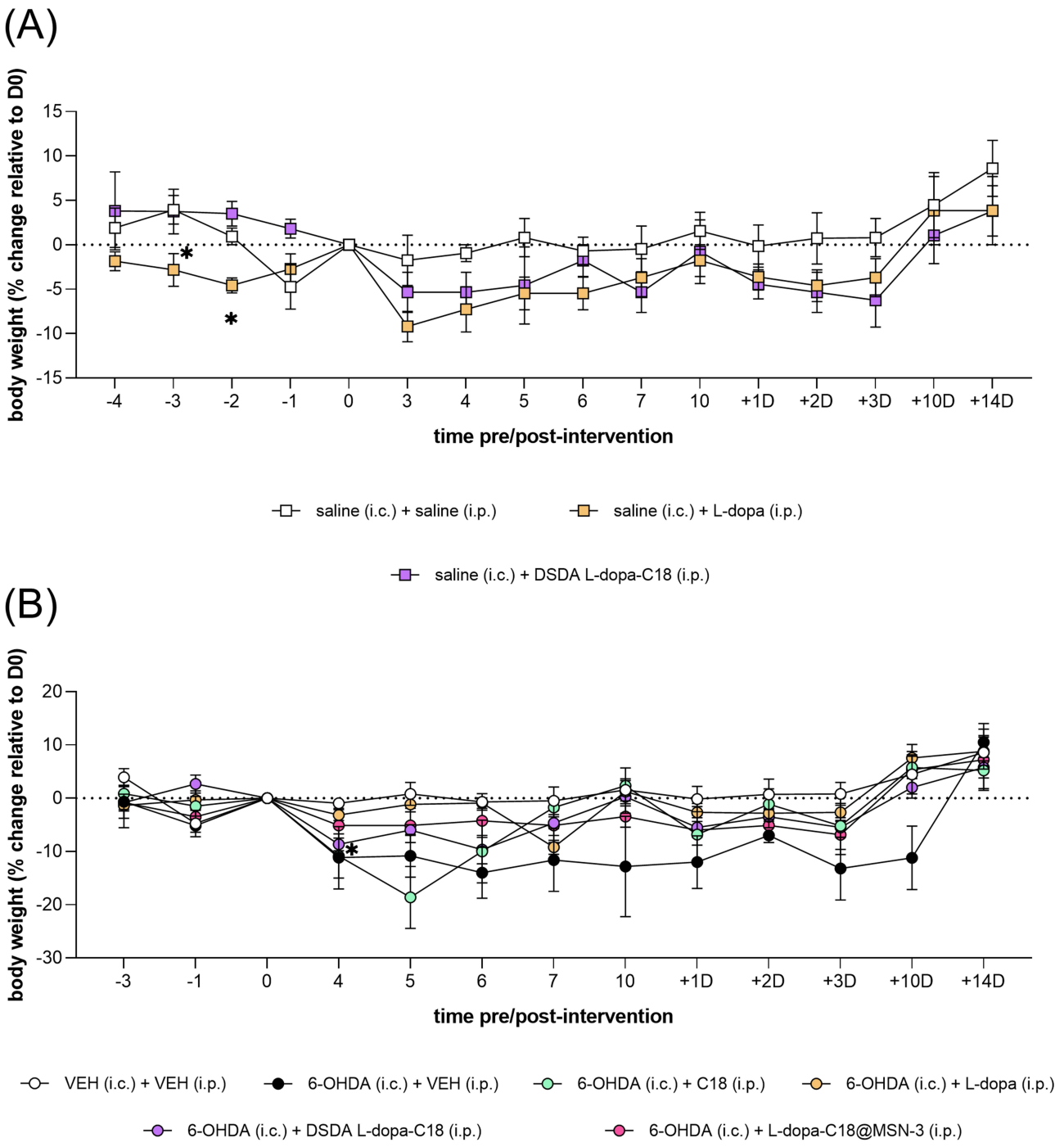

Figure 7 Body weight change relative to day 0 in (**A**) saline (i.c.) and (**B**) 6-OHDA (i.c.) animals. *P<0.05 vs sham (saline, i.p)., two-way ANOVA followed by Dunnett's Multiple comparisons test.

model of Parkinson's disease. The synthesis parameters and alkyl chain length were systematically optimized to generate an MSN formulation with favorable size, morphology and drug content for in vivo testing. Of the materials developed, L-dopa-C18@MSN-3 was identified as the optimal candidate, demonstrating high L-dopa loading (approximately 22%) whilst maintaining favorable textural properties.

Release studies highlighted a clear distinction in the mechanisms of release between DSDA-templated MSNs and conventional adsorption into mesopores. L-dopa-C18@MSN-3 exhibited sustained, non-plateauing release for at least 14

https://doi.org/10.2147/IJN.S545116

days at physiological pH. In contrast, the conventionally loaded reference material released most of its payload within 24 hours, consistent with rapid solvent access to the surface-adsorbed drug. Together with in vitro biocompatibility and FBS-mediated biodegradation data, these findings support the suitability of the DSDA platform for controlled L-dopa delivery.

In vivo, a single intraperitoneal dose of 25 mg/kg L-dopa equivalent of L-dopa-C18@MSN-3 reduced spontaneous rotational behavior in 6-OHDA-lesioned mice, demonstrating greater durability than free L-dopa at the same dose. The L-dopa-C10 analogue did not improve behavior, which aligns with the rationale of testing different chain lengths. These results demonstrate that DSDA-templated MSNs can translate their sustained-release profile into meaningful, long-lasting functional benefits in vivo, showing that DSDA-based encapsulation of L-dopa is a viable strategy for sustained drug delivery in chronic conditions such as Parkinson's disease. Further studies are needed to advance towards clinical translation, investigating the pharmacokinetics, biodistribution, chronic toxicity and long-term safety profile of these nanoformulations, as well as optimizing the dosing regimen and administration protocols.

Ethics Approval

All animal procedures were designed and conducted in accordance with a protocol approved by the Ethical Committee of Universidad Rey Juan Carlos and by the Autonomous Region of Madrid (PROEX 247.4/22) and followed the guidelines for the Care and Use of Laboratory Animals of the European Union Directive (2010/63/EU) and Spanish regulations (Law 32/2007, RD 53/2013 and order ECC/566/2015).

Acknowledgments

The authors would like to thank Mrs. Carmen Merino for her technical assistance in the Pharmacology Laboratory at Universidad Rey Juan Carlos.

Funding

The financial support by the Spanish Agencia Estatal de Investigación/Ministerio de Ciencia e Innovación MCIN/AEI/10.13039/501100011033 (Grants No. PID2021-1252160B-100 and PID2024-1604280B-100) is gratefully acknowledged. In addition, this work was supported with research grant IMPULSO, URJC's Own Program for the Promotion and Development of Research for young doctors (2022-REGING-94948) awarded to AM.

Disclosure

The authors declare that there is no conflict of interest upon the publication of this manuscript.

References

1. Feigin VL, Nichols E, Alam T, et al. GBD dementia collaborators, global, regional, and national burden of neurological disorders, 1990–2016: a systematic analysis for the global burden of disease study 2016. *Lancet Neurol*. 2019;18:459–480. doi:10.1016/S1474-4422(18)30499-X
2. Wen JH, He XH, Feng ZS, Li DY, Tang JX, Liu HF. Cellular protein aggregates: formation, biological effects, and ways of elimination. *IJMS*. 2023;24(10):8593. doi:10.3390/ijms24108593
3. Ding C, Chen Y, Chen X, et al. Global, regional, and national burden and attributable risk factors of neurological disorders: the global burden of disease study 1990–2019. *Front Public Health*. 2022:10. 10.3389/fpubh.2022.952161.
4. Dorsey ER, Elbaz A, Nichols E, et al. Global, regional, and national burden of parkinson's disease, 1990–2016: a systematic analysis for the global burden of disease study 2016. *Lancet Neurol*. 2018;17(11):939–953. doi:10.1016/S1474-4422(18)30295-3
5. Domingues R, Sant'Anna R, Da Fonseca ACC, Robbs BK, Foguel D, Outeiro TF. Extracellular alpha-synuclein: sensors, receptors, and responses. *Neurobiol Dis*. 2022;168:105696. doi:10.1016/j.nbd.2022.105696
6. Wilson DM, Cookson MR, Van Den Bosch L, Zetterberg H, Holtzman DM, Dewachter I. Hallmarks of neurodegenerative diseases. *Cell*. 2023;186(4):693–714. doi:10.1016/j.cell.2022.12.032
7. Poewe W, Seppi K, Tanner CM, et al. Parkinson disease. *Nat Rev Dis Primers*. 2017;3(1):17013. doi:10.1038/nrdp.2017.13
8. Yamada K, Iwatsubo T. Extracellular α-synuclein levels are regulated by neuronal activity. *Mol Neurodegeneration*. 2018;13(1):9. doi:10.1186/s13024-018-0241-0
9. Bloem BR, Okun MS, Klein C. Parkinson's disease. *Lancet*. 2021;397(10291):2284–2303. doi:10.1016/S0140-6736(21)00218-X
10. Vaugoyeau M. Axial rotation in Parkinson's disease. *J Neurol Neurosurg*. 2006;77(7):815–821. doi:10.1136/jnnp.2004.050666
11. Cools R. Dopaminergic modulation of cognitive function-implications for l-DOPA treatment in Parkinson's disease. *Neurosci Biobehav Rev*. 2006;30(1):1–23. doi:10.1016/j.neubiorev.2005.03.024
12. Jost WH. Dopamine agonists in the treatment of Parkinson's disease: the show must go on. *J Neural Transm*. 2024;131(12):1471–1480. doi:10.1007/s00702-024-02825-8

13. LeWitt PA, Stocchi F, Arkadir D, et al. The pharmacokinetics of continuous subcutaneous levodopa/carbidopa infusion: findings from the ND0612 clinical development program. *Front Neurol*. 2022;13:1036068. doi:10.3389/fneur.2022.1036068
14. Stacy M. The wearing-off phenomenon and the use of questionnaires to facilitate its recognition in Parkinson's disease. *J Neural Transm*. 2010;117 (7):837–846. doi:10.1007/s00702-010-0424-5
15. McFarthing K, Buff S, Rafaloff G, et al. Parkinson's disease drug therapies in the clinical trial pipeline: 2024 update. *JPD*. 2024;14(5):899–912. doi:10.3233/JPD-240272
16. Espay AJ, Pagan FL, Walter BL, et al. Optimizing extended-release carbidopa/levodopa in Parkinson disease: consensus on conversion from standard therapy. *Neur Clin Pract*. 2017;7(1):86–93. doi:10.1212/CPJ.0000000000000316
17. Olanow CW, Espay AJ, Stocchi F, et al. continuous subcutaneous levodopa delivery for parkinson's disease: a randomized study. *JPD*. 2021;11 (1):177–186. doi:10.3233/JPD-202285
18. Honig H, Antonini A, Martinez-Martin P, et al. Intrajejunal levodopa infusion in Parkinson's disease: a pilot multicenter study of effects on nonmotor symptoms and quality of life. *Mov Disord*. 2009;24(10):1468–1474. doi:10.1002/mds.22596
19. Poewe W, Antonini A. Novel formulations and modes of delivery of levodopa. *Mov Disord*. 2015;30(1):114–120. doi:10.1002/mds.26078
20. García-Pardo J, Novio F, Nador F, et al. Bioinspired theranostic coordination polymer nanoparticles for intranasal dopamine replacement in parkinson's disease. *ACS Nano*. 2021;15(5):8592–8609. doi:10.1021/acsnano.1c00453
21. Arıca B, Kaş HS, Moghdam A, Akalan N, Hıncal AA. Carbidopa/levodopa-loaded biodegradable microspheres: in vivo evaluation on experimental Parkinsonism in rats. *J Control Release*. 2005;102(3):689–697. doi:10.1016/j.jconrel.2004.11.004
22. Yeni Y, Genc S, Ertugrul MS, et al. Neuroprotective effects of L-Dopa-modified zinc oxide nanoparticles on the rat model of 6-OHDA-ınduced Parkinson's disease. *Sci Rep*. 2024;14(1):19077. doi:10.1038/s41598-024-69324-4
23. Narayan R, Nayak U, Raichur A, Garg S. Mesoporous silica nanoparticles: a comprehensive review on synthesis and recent advances. *Pharmaceutics*. 2018;10(3):118. doi:10.3390/pharmaceutics10030118
24. Zhou Y, Quan G, Wu Q, et al. Mesoporous silica nanoparticles for drug and gene delivery. *Acta Pharmaceutica Sinica B*. 2018;8(2):165–177. doi:10.1016/j.apsb.2018.01.007
25. Manzano M, Vallet-Regí M. Mesoporous silica nanoparticles for drug delivery. *Adv Funct Mater*. 2020;30(2):1902634. doi:10.1002/ adfm.201902634
26. Pandey PK, Sharma AK, Rani S, et al. MCM-41 nanoparticles for brain delivery: better choline-esterase and amyloid formation inhibition with improved kinetics. *ACS Biomater Sci Eng*. 2018;4(8):2860–2869. doi:10.1021/acsbiomaterials.8b00335
27. Giri S, Trewyn BG, Stellmaker MP, Lin VS-Y. Stimuli-responsive controlled-release delivery system based on mesoporous silica nanorods capped with magnetic nanoparticles. *Angew Chem Int Ed*. 2005;44(32):5038–5044. doi:10.1002/anie.200501819
28. Cheng CS, Liu TP, Chien FC, Mou CY, Wu SH, Chen YP. Codelivery of plasmid and curcumin with mesoporous silica nanoparticles for promoting neurite outgrowth. *ACS Appl Mater Interfaces*. 2019;11(17):15322–15331. doi:10.1021/acsami.9b02797
29. Charnay C, Bégu S, Tourné-Péteilh C, Nicole L, Lerner DA, Devoisselle JM. Inclusion of ibuprofen in mesoporous templated silica: drug loading and release property. *Eur J Pharm Biopharm*. 2004;57(3):533–540. doi:10.1016/j.ejpb.2003.12.007
30. Morales V, Idso MN, Balabasquer M, Chmelka B, García-Muñoz RA. Correlating surface-functionalization of mesoporous silica with adsorption and release of pharmaceutical guest species. *J Phys Chem C*. 2016;120(30):16887–16898. doi:10.1021/acs.jpcc.6b06238
31. Morales V, Martín A, Ortiz-Bustos J, Sanz R, García-Muñoz RA. Effect of the dual incorporation of fullerene and polyethyleneimine moieties into SBA-15 materials as platforms for drug delivery. *J Mater Sci*. 2019;54(17):11635–11653. doi:10.1007/s10853-019-03708-0
32. García-Muñoz RA, Morales V, Linares M, González PE, Sanz R, Serrano DP. Influence of the structural and textural properties of ordered mesoporous materials and hierarchical zeolitic supports on the controlled release of methylprednisolone hemisuccinate. *J Mater Chem B*. 2014;2 (45):7996–8004. doi:10.1039/C4TB00089G
33. Vallet-Regí M. Ordered mesoporous materials in the context of drug delivery systems and bone tissue engineering. *Chem a Eur J*. 2006;12 (23):5934–5943. doi:10.1002/chem.200600226
34. Kovtareva S, Kusepova L, Tazhkenova G, Mashan T, Bazarbaeva K, Kopishev E. Surface modification of mesoporous silica nanoparticles for application in targeted delivery systems of antitumour drugs. *Polymers*. 2024;16(8):1105. doi:10.3390/polym16081105
35. Lu D, Lei J, Wang L, Zhang J. Multifluorescently traceable nanoparticle by a single-wavelength excitation with color-related drug release performance. *J Am Chem Soc*. 2012;134(21):8746–8749. doi:10.1021/ja301691j
36. Parambadath S, Rana VK, Zhao D, Ha CS. N,N′-diureylenepiperazine-bridged periodic mesoporous organosilica for controlled drug delivery. *Microporous Mesoporous Mater*. 2011;141(1–3):94–101. doi:10.1016/j.micromeso.2010.10.051
37. Sábio RM, Meneguin AB, Ribeiro TC, Silva RR, Chorilli M. New insights towards mesoporous silica nanoparticles as a technological platform for chemotherapeutic drugs delivery. *Int J pharm*. 2019;564:379–409. doi:10.1016/j.ijpharm.2019.04.067
38. Hoshyar N, Gray S, Han H, Bao G. The effect of nanoparticle size on *in vivo* pharmacokinetics and cellular interaction. *Nanomedicine*. 2016;11 (6):673–692. doi:10.2217/nnm.16.5
39. Mohamed F, Oo MK, Chatterjee B, Alallam B. Biocompatible supramolecular mesoporous silica nanoparticles as the next-generation drug delivery system. *Front Pharmacol*. 2022;13:886981. doi:10.3389/fphar.2022.886981
40. Mitchell MJ, Billingsley MM, Haley RM, Wechsler ME, Peppas NA, Langer R. Engineering precision nanoparticles for drug delivery. *Nat Rev Drug Discov*. 2021;20(2):101–124. doi:10.1038/s41573-020-0090-8
41. Ragnaill MN, Brown M, Ye D, et al. Internal benchmarking of a human blood–brain barrier cell model for screening of nanoparticle uptake and transcytosis. *Eur J Pharm Biopharm*. 2011;77(3):360–367. doi:10.1016/j.ejpb.2010.12.024
42. Janjua TI, Ahmed-Cox A, Meka AK, et al. Facile synthesis of lactoferrin conjugated ultra small large pore silica nanoparticles for the treatment of glioblastoma. *Nanoscale*. 2021;13(40):16909–16922. doi:10.1039/D1NR03553C
43. Hanada S, Fujioka K, Inoue Y, Kanaya F, Manome Y, Yamamoto K. Cell-based in vitro blood–brain barrier model can rapidly evaluate nanoparticles' brain permeability in association with particle size and surface modification. *IJMS*. 2014;15(2):1812–1825. doi:10.3390/ijms15021812
44. López T, Esquivel D, Mendoza-Díaz G, Ortiz-Islas E, González RD, Novaro O. L-DOPA stabilization on sol–gel silica to be used as neurological nanoreservoirs: structural and spectroscopic studies. *Mater Lett*. 2015;161:160–163. doi:10.1016/j.matlet.2015.08.015
45. Kiss T, Katona G, Mérai L, et al. Development of a hydrophobicity-controlled delivery system containing levodopa methyl ester hydrochloride loaded into a mesoporous silica. *Pharmaceutics*. 2021;13(7):1039. doi:10.3390/pharmaceutics13071039

46. Swar S, Máková V, Stibor I. Effectiveness of diverse mesoporous silica nanoparticles as potent vehicles for the drug L-DOPA. *Materials*. 2019;12(19):3202. doi:10.3390/ma12193202
47. Garcia-Munoz R, McConnell J, Morales V, Sanz R. Designing nanocarriers to overcome the limitations in conventional drug administration for Parkinson's disease. *Neural Regen Res*. 2022;17(8):1743. doi:10.4103/1673-5374.332143
48. Morales V, Pérez-Garnes M, Balabasquer M, González-Casablanca J, García-Muñoz RA. Oil-in-water synthesis of hollow-shell mesoporous peapod-like silicates: electron microscopy insights. *Microporous Mesoporous Mater*. 2018;264:43–54. doi:10.1016/j.micromeso.2018.01.005
49. Morales V, Gutiérrez-Salmerón M, Balabasquer M, et al. New drug-structure-directing agent concept: inherent pharmacological activity combined with templating solid and hollow-shell mesostructured silica nanoparticles. *Adv Funct Mater*. 2016;26(40):7291–7303. doi:10.1002/adfm.201505073
50. López-Ruiz M, Navas F, Fernández-García P, et al. L-arginine-containing mesoporous silica nanoparticles embedded in dental adhesive (Arg@MSN@DAdh) for targeting cariogenic bacteria. *J Nanobiotechnol*. 2022;20(1):502. doi:10.1186/s12951-022-01714-0
51. Martinez-Erro S, Navas F, Romaní-Cubells E, et al. Kidney-protector lipidic cilastatin derivatives as structure-directing agents for the synthesis of mesoporous silica nanoparticles for drug delivery. *IJMS*. 2021;22(15):7968. doi:10.3390/ijms22157968
52. Morales V, McConnell J, Pérez-Garnes M, Almendro N, Sanz R, García-Muñoz RA. Dopa release from mesoporous silica nanoparticles engineered through the concept of drug-structure-directing agents for Parkinson's disease. *J Mater Chem B*. 2021;9(20):4178–4189. doi:10.1039/D1TB00481F
53. Romaní-Cubells E, Martinez-Erro S, Morales V, Van Grieken R, García Muñoz RA, Sanz R. Mitoxantrone-derivative drug structure-directing agent for the synthesis of magnetic mesoporous silica nanoparticles for breast cancer treatment. *ACS Appl Nano Mater*. 2024;7(11):12376–12386. doi:10.1021/acsanm.4c00393
54. Jiménez-Díez D, Fernández-García P, Navas F, et al. Antimicrobial and physico-mechanical properties of a universal adhesive loaded with L-arginine-containing mesoporous silica nanoparticles (ArgC18@MSNs). *Dent Mater*. 2025;41(11):1465–1477. doi:10.1016/j.dental.2025.08.004
55. Scheline RR, Santesson J, Tibell L, et al. A Rapid Synthesis of 3-O-Methylgallic Acid. *Acta Chem Scand*. 1966;20:1182. doi:10.3891/acta.chem.scand.20-1182
56. Wang J, Xiao Q, Zhou H, et al. Budded, mesoporous silica hollow spheres: hierarchical structure controlled by kinetic self-assembly. *Adv Mater*. 2006;18(24):3284–3288. doi:10.1002/adma.200601321
57. Di L, Kerns EH, Fan K, McConnell OJ, Carter GT. High throughput artificial membrane permeability assay for blood–brain barrier. *Eur J Med Chem*. 2003;38(3):223–232. doi:10.1016/S0223-5234(03)00012-6
58. García MM, Molina-álvarez M, Rodríguez-Rivera C, et al. Antinociceptive and modulatory effect of pathoplastic changes in spinal glia of a TLR4/CD14 blocking molecule in two models of pain in rat. *Biomed Pharmacother*. 2022;150:112986. doi:10.1016/j.biopha.2022.112986
59. Kresge CT, Leonowicz ME, Roth WJ, Vartuli JC, Beck JS. Ordered mesoporous molecular sieves synthesized by a liquid-crystal template mechanism. *Nature*. 1992;359(6397):710–712. doi:10.1038/359710a0
60. Pogorelov VM, Martini ML, Jin J, Wetsel WC, Caron MG. Dopamine-Depleted Dopamine Transporter Knockout (DDD) Mice: dyskinesia with L-DOPA and Dopamine D1 Agonists. *Biomolecules*. 2023;13(11):1658. doi:10.3390/biom13111658
61. Djaldetti R, Atlas D, Melamed E. Effect of subcutaneous administration of levodopa ethyl ester, a soluble prodrug of levodopa, on dopamine metabolism in rodent striatum: implication for treatment of parkinson's disease. *Clin Neuropharmacol*. 1996;19(1):65–71. doi:10.1097/00002826-199619010-00005
62. Nair A, Jacob S. A simple practice guide for dose conversion between animals and human. *J Basic Clin Pharm*. 2016;7(2):27. doi:10.4103/0976-0105.177703
63. Ayieko P, Ntoburi S, Wagai J, et al. A multifaceted intervention to implement guidelines and improve admission paediatric care in kenyan district hospitals: a cluster randomised trial. *PLoS Med*. 2011;8(4):e1001018. doi:10.1371/journal.pmed.1001018
64. Da Conceição FSL, Ngo-Abdalla S, Houzel JC, Rehen SK. Murine model for parkinson's disease: from 6-oh dopamine lesion to behavioral test. *JoVE*. 2010;(35):1376. doi:10.3791/1376
65. Yu H, Liu X, Chen B, et al. The Neuroprotective Effects of the CB2 Agonist GW842166x in the 6-OHDA Mouse Model of Parkinson's Disease. *Cells*. 2021;10(12):3548. doi:10.3390/cells10123548
66. Boix J, Padel T, Paul G. A partial lesion model of Parkinson's disease in mice – characterization of a 6-OHDA-induced medial forebrain bundle lesion. *Behav Brain Res*. 2015;284:196–206. doi:10.1016/j.bbr.2015.01.053
67. Robinson TE, Becker JB. The rotational behavior model: asymmetry in the effects of unilateral 6-OHDA lesions of the substantia nigra in rats. *Brain Res*. 1983;264(1):127–131. doi:10.1016/0006-8993(83)91129-0
68. Liao C-H, Chen S-Y, Kuo J-S, Pang C-Y. Reduction of motor disorder in 6-OHDA-induced severe parkinsonism rats by post treatment with granulocyte-colony stimulating factor. *Chin J Physiol*. 2013;56(3). doi:10.4077/CJP.2013.BAB125
69. Alvarsson A, Zhang X, Stan TL, et al. Modulation by trace amine-associated receptor 1 of experimental parkinsonism, l-DOPA responsivity, and glutamatergic neurotransmission. *J Neurosci*. 2015;35(41):14057–14069. doi:10.1523/JNEUROSCI.1312-15.2015
70. Lerner RP, Francardo V, Fujita K, et al. Levodopa-induced abnormal involuntary movements correlate with altered permeability of the blood-brain-barrier in the basal ganglia. *Sci Rep*. 2017;7(1):16005. doi:10.1038/s41598-017-16228-1
71. Huttunen J, Peltokangas S, Gynther M, et al. l-type amino acid transporter 1 (LAT1/Lat1)-utilizing prodrugs can improve the delivery of drugs into neurons, astrocytes and microglia. *Sci Rep*. 2019;9(1):12860. doi:10.1038/s41598-019-49009-z
72. Peura L, Malmioja K, Huttunen K, et al. Design, SYNTHESIS AND BRAIN UPtake of LAT1-targeted amino acid prodrugs of dopamine. *Pharm Res*. 2013;30(10):2523–2537. doi:10.1007/s11095-012-0966-3
73. Hachem M, Belkouch M, Lo Van A, Picq M, Bernoud-Hubac N, Lagarde M. Brain targeting with docosahexaenoic acid as a prospective therapy for neurodegenerative diseases and its passage across blood brain barrier. *Biochimie*. 2020;170:203–211. doi:10.1016/j.biochi.2020.01.013
74. Furtado D, Björnmalm M, Ayton S, Bush AI, Kempe K, Caruso F. Overcoming the blood–brain barrier: the role of nanomaterials in treating neurological diseases. *Adv Mater*. 2018;30(46):1801362. doi:10.1002/adma.201801362
75. Jiang W, Lv L, Zhou S, et al. Simultaneous determination of l-dopa and its prodrug (S)-4-(2-acetamido-3-ethoxy-3-oxopropyl)-1,2-phenylene diacetate in rat plasma by high-performance liquid chromatography–tandem mass spectrometry and its application in a pharmacokinetic study. *J Pharmaceut Biomed Anal*. 2010;53(3):751–754. doi:10.1016/j.jpba.2010.05.003
76. Möller K, Kobler J, Bein T. Colloidal Suspensions of Nanometer-Sized Mesoporous Silica. *Adv Funct Mater*. 2017;17(4):499–664. doi:10.1002/adfm.200600578

77. Cauda V, Schlossbauer A, Bein T. Bio-degradation study of colloidal mesoporous silica nanoparticles: effect of surface functionalization with organo-silanes and poly(ethylene glycol). *Microporous Mesoporous Mater*. 2010;132(1–2):60–71. doi:10.1016/j.micromeso.2009.11.015
78. Halder J, Pradhan D, Kar B, Ghosh G, Rath G. Nanotherapeutics approaches to overcome P-glycoprotein-mediated multi-drug resistance in cancer. *Nanomed Nanotechnol Biol Med*. 2022;40:102494. doi:10.1016/j.nano.2021.102494
79. Basma AN, Morris EJ, Nicklas WJ, Geller HM. DOPA Cytotoxicity to PC12 cells in culture is via its autoxidation. *J Neurochem*. 1995;64 (2):825–832. doi:10.1046/j.1471-4159.1995.64020825.x
80. Ziv I, Zilkha-Falb R, Offen D, Shirvan A, Barzilai A, Melamed E. Levodopa induces apoptosis in cultured neuronal cells—A possible accelerator of nigrostriatal degeneration in Parkinson's disease? *Mov Disord*. 1997;12(1):17–23. doi:10.1002/mds.870120105
81. Su R, Zhen J, Wang W, Zhang J, Zhen Y, Wang X. Time-course behavioral features are correlated with Parkinson's disease-associated pathology in a 6-hydroxydopamine hemiparkinsonian rat model. *Mol Med Rep*. 2017. doi:10.3892/mmr.2017.8277
82. Thiele SL, Warre R, Nash JE. Development of a Unilaterally-lesioned 6-OHDA mouse model of parkinson's disease. *JoVE*. 2012;(60):3234. doi:10.3791/3234
83. Truong L, Allbutt H, Kassiou M, Henderson JM. Developing a preclinical model of Parkinson's disease: a study of behaviour in rats with graded 6-OHDA lesions. *Behav Brain Res*. 2006;169(1):1–9. doi:10.1016/j.bbr.2005.11.026
84. Rentsch P, Stayte S, Morris GP, Vissel B. Time dependent degeneration of the nigrostriatal tract in mice with 6-OHDA lesioned medial forebrain bundle and the effect of activin A on l-Dopa induced dyskinesia. *BMC Neurosci*. 2019;20(1):5. doi:10.1186/s12868-019-0487-7
85. Da Cunha C, Wietzikoski EC, Ferro MM, et al. Hemiparkinsonian rats rotate toward the side with the weaker dopaminergic neurotransmission. *Behav Brain Res*. 2008;189(2):364–372. doi:10.1016/j.bbr.2008.01.012
86. Bagga V, Dunnett SB, Fricker RA. The 6-OHDA mouse model of Parkinson's disease – terminal striatal lesions provide a superior measure of neuronal loss and replacement than median forebrain bundle lesions. *Behav Brain Res*. 2015;288:107–117. doi:10.1016/j.bbr.2015.03.058
87. Tronci E, Shin E, Björklund A, Carta M. Amphetamine-induced rotation and l-DOPA-induced dyskinesia in the rat 6-OHDA model: a correlation study. *Neurosci Res*. 2012;73(2):168–172. doi:10.1016/j.neures.2012.03.004
88. Mottaghi S, Kohl S, Biemann D, et al. Bilateral intracranial beta activity during forced and spontaneous movements in a 6-OHDA hemi-PD rat model. *Front Neurosci*. 2021;15:700672. doi:10.3389/fnins.2021.700672
89. Sun X, Li X, Zhang L, et al. Longitudinal assessment of motor function following the unilateral intrastriatal 6-hydroxydopamine lesion model in mice. *Front Behav Neurosci*. 2022;16:982218. doi:10.3389/fnbeh.2022.982218
90. De Carvalho MB, Teixeira-Silva B, Marques SA, et al. NMDA receptor remodeling and nNOS activation in mice after unilateral striatal injury with 6-OHDA. *Heliyon*. 2024;10(14):e34120. doi:10.1016/j.heliyon.2024.e34120
91. Mendes-Pinheiro B, Soares-Cunha C, Marote A, et al. Unilateral intrastriatal 6-hydroxydopamine lesion in mice: a closer look into non-motor phenotype and glial response. *IJMS*. 2021;22(21):11530. doi:10.3390/ijms222111530